
FLamby: Datasets and Benchmarks for Cross-Silo Federated Learning in Realistic Healthcare Settings

Jean Ogier du Terrail¹ Samy-Safwan Ayed² Edwige Cyffers³ Felix Grimberg⁴
 Chaoyang He⁵ Regis Loeb¹ Paul Mangold³ Tanguy Marchand¹
 Othmane Marfoq² Erum Mushtaq⁶ Boris Muzellec¹ Constantin Philippenko⁷
 Santiago Silva² Maria Teleńczuk¹ Shadi Albarqouni^{8,9} Salman Avestimehr^{5,6}
 Aurélien Bellet³ Aymeric Dieuleveut⁷ Martin Jaggi⁴
 Sai Praneeth Karimireddy¹⁰ Marco Lorenzi² Giovanni Neglia² Marc Tommasi³
 Mathieu Andreux¹

¹Owkin, Inc, ²Inria, Université Côte d’Azur, Sophia Antipolis, France

³Univ. Lille, Inria, CNRS, Centrale Lille, UMR 9189 - CRIStAL, F-59000 Lille, France

⁴EPFL ⁵FedML, Inc. ⁶University of Southern California

⁷CMAP, UMR 7641, École Polytechnique, Institut Polytechnique de Paris

⁸University Hospital Bonn ⁹Helmholtz Munich ¹⁰University of California, Berkeley

{jean.du-terrail, regis.loeb, tanguy.marchand, boris.muzellec,
 maria.telenczuk, mathieu.andreux}@owkin.com, {samy-safwan.ayed,
 edwige.cyffers, paul.mangold, othamne.marfoq,
 santiago-smith.silva-rincon, aurelien.bellet,
 marco.lorenzi, giovanni.neglia, marc.tommasi}@inria.fr
 {felix.grimberg, martin.jaggi}@epfl.ch,
 ch@fedml.ai, {emushtaq, avestime}@usc.edu,
 {constantin.philippenko, aymeric.dieuleveut}@polytechnique.edu,
 shadi.albarqouni@ukbonn.de, sp.karimireddy@berkeley.edu

Abstract

Federated Learning (FL) is a novel approach enabling several clients holding sensitive data to collaboratively train machine learning models, without centralizing data. The cross-silo FL setting corresponds to the case of few (2–50) reliable clients, each holding medium to large datasets, and is typically found in applications such as healthcare, finance, or industry. While previous works have proposed representative datasets for cross-device FL, few realistic healthcare cross-silo FL datasets exist, thereby slowing algorithmic research in this critical application. In this work, we propose a novel cross-silo dataset suite focused on healthcare, FLamby (Federated Learning AMple Benchmark of Your cross-silo strategies), to bridge the gap between theory and practice of cross-silo FL. FLamby encompasses 7 healthcare datasets with natural splits, covering multiple tasks, modalities, and data volumes, each accompanied with baseline training code. As an illustration, we additionally benchmark standard FL algorithms on all datasets. Our flexible and modular suite allows researchers to easily download datasets, reproduce results and re-use the different components for their research. FLamby is available at www.github.com/owkin/flamby.

1 Introduction

Recently it has become clear that, in many application fields, impressive machine learning (ML) task performance can be reached by scaling the size of both ML models and their training data while

keeping existing well-performing architectures mostly unaltered [118, 74, 21, 109]. In this context, it is often assumed that massive training datasets can be collected and centralized in a single client in order to maximize performance. However, in many application domains, data collection occurs in distinct sites (further referred to as clients, e.g., mobile devices or hospitals), and the resulting local datasets cannot be shared with a central repository or data center due to privacy or strategic concerns [39, 15].

To enable cooperation among clients given such constraints, Federated Learning (FL) [97, 71] has emerged as a viable alternative to train models across data providers without sharing sensitive data. While initially developed to enable training across a large number of small clients, such as smartphones or Internet of Things (IoT) devices, it has been then extended to the collaboration of fewer and larger clients, such as banks or hospitals. The two settings are now respectively referred to as *cross-device* FL and *cross-silo* FL, each associated with specific use cases and challenges [71].

On the one hand, cross-device FL leverages edge devices such as mobile phones and wearable technologies to exploit data distributed over billions of data sources [97, 13, 11, 101]. Therefore, it often requires solving problems related to edge computing [51, 85, 129], participant selection [71, 131, 20, 42], system heterogeneity [71], and communication constraints such as low network bandwidth and high latency [113, 91, 49]. On the other hand, cross-silo initiatives enable to untap the potential of large datasets previously out of reach. This is especially true in healthcare, where the emergence of federated networks of private and public actors [112, 115, 103], for the first time, allows scientists to gather enough data to tackle open questions on poorly understood diseases such as triple negative breast cancer [37] or COVID-19 [31]. In cross-silo applications, each silo has large computational power, a relatively high bandwidth, and a stable network connection, allowing it to participate to the whole training phase. However, cross-silo FL is typically characterized by high inter-client dataset heterogeneity and biases of various types across the clients [103, 37].

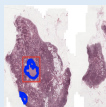

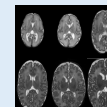
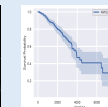
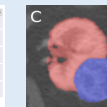
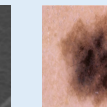
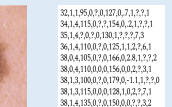
As we show in Section 2, publicly available datasets for the cross-silo FL setting are scarce. As a consequence, researchers usually rely on heuristics to artificially generate heterogeneous data partitions from a single dataset and assign them to hypothetical clients. Such heuristics might fall short of replicating the complexity of natural heterogeneity found in real-world datasets. The example of digital histopathology [126], a crucial data type in cancer research, illustrates the potential limitations of such synthetic partition methods. In digital histopathology, tissue samples are extracted from patients, stained, and finally digitized. In this process, known factors of data heterogeneity across hospitals include patient demographics, staining techniques, storage methodologies of the physical slides, and digitization processes [69, 43, 57]. Although staining normalization [79, 32] has seen recent progress, mitigating this source of heterogeneity, the other highlighted sources of heterogeneity are difficult to replicate with synthetic partitioning [57] and some may be unknown, which calls for actual cross-silo cohort experiments. This observation is also valid for many other application domains, e.g. radiology [50], dermatology [7], retinal images [7] and more generally computer vision [122].

In order to address the lack of realistic cross-silo datasets, we propose FLamby, an open source cross-silo federated dataset suite with natural partitions focused on healthcare, accompanied by code examples, and benchmarking guidelines. Our ambition is that FLamby becomes the reference benchmark for cross-silo FL, as LEAF [16] is for cross-device FL. To the best of our knowledge, apart from some promising isolated works to build realistic cross-silo FL datasets (see Section 2), our work is the first standard benchmark allowing to systematically study healthcare cross-silo FL on different data modalities and tasks.

To summarize, our contributions are threefold:

1. We build an open-source federated cross-silo healthcare dataset suite including 7 datasets. These datasets cover different tasks (classification / segmentation / survival) in multiple application domains and with different data modalities and scale. Crucially, all datasets are partitioned using natural splits.
2. We provide guidelines to help compare FL strategies in a fair and reproducible manner, and provide illustrative results for this benchmark.
3. We make open-source code accessible for benchmark reproducibility and easy integration in different FL frameworks, but also to allow the research community to contribute to FLamby development, by adding more datasets, benchmarking types and FL strategies.

Table 1: Overview of the datasets, tasks, metrics and baseline models in FLamby. For Fed-Camelyon16 the two different sizes refer to the size of the dataset before and after tiling.

Dataset	Fed-Camelyon16	Fed-LIDC-IDRI	Fed-IXI	Fed-TCGA-BRCA	Fed-KITS2019	Fed-ISIC2019	Fed-Heart-Disease
Input (x)	Slides	CT-scans	T1WI	Patient info.	CT-scans	Dermoscopy	Patient info.
Preprocessing	Matter extraction + tiling	Patch Sampling	Registration	None	Patch Sampling	Various image transforms	Removing missing data
Task type	binary classification	3D segmentation	3D segmentation	survival	3D segmentation	multi-class classification	binary classification
Prediction (y)	Tumor on slide	Lung Nodule Mask	Brain mask	Risk of death	Kidney and tumor masks	Melanoma class	Heart disease
Center extraction	Hospital	Scanner Manufacturer	Hospital	Group of Hospitals	Group of Hospitals	Hospital	Hospital
Thumbnails							
Original paper	Litjens <i>et al.</i> 2018	Armato <i>et al.</i> 2011	Perez <i>et al.</i> 2021	Liu <i>et al.</i> 2018	Heller <i>et al.</i> 2019	Tschandl <i>et al.</i> 2018 / Codella <i>et al.</i> 2017 / Combalia <i>et al.</i> 2019	Janosi <i>et al.</i> 1988
# clients	2	4	3	6	6	6	4
# examples	399	1,018	566	1,088	96	23, 247	740
# examples per center	239, 150	670, 205, 69, 74	311, 181, 74	311, 196, 206, 162, 162, 51	12, 14, 12, 12, 16, 30	12413, 3954, 3363, 225, 819, 439	303, 261, 46, 130
Model	DeepMIL [64]	Vnet [98, 100]	3D U-net [22]	Cox Model [30]	nnU-Net [67]	efficientnet [119] + linear layer	Logistic Regression
Metric	AUC	DICE	DICE	C-index	DICE	Balanced Accuracy	Accuracy
Size	50G (850G total)	115G	444M	115K	54G	9G	40K
Image resolution	0.5 μm / pixel	$\sim 1.0 \times 1.0 \times 1.0$ mm / voxel	$\sim 1.0 \times 1.0 \times 1.0$ mm / voxel	NA	$\sim 1.0 \times 1.0 \times 1.0$ mm / voxel	~ 0.02 mm / pixel	NA
Input dimension	10,000 x 2048	128 x 128 x 128	48 x 60 x 48	39	64 x 192 x 192	200 x 200 x 3	13

This paper is organized as follows. Section 2 reviews existing FL datasets and benchmarks, as well as client partition methods used to artificially introduce data heterogeneity. In Section 3, we describe our dataset suite in detail, notably its structure and the intrinsic heterogeneity of each federated dataset. Finally, we define a benchmark of several FL strategies on all datasets and provide results thereof in Section 4.

2 Related Work

In FL, data is collected locally in clients in different conditions and without coordination. As a consequence, clients’ datasets differ both in size (unbalanced) and in distribution (non-IID) [97]. The resulting *statistical heterogeneity* is a fundamental challenge in FL [82, 71], and it is necessary to take it into consideration when evaluating FL algorithms. Most FL papers simulate statistical heterogeneity by artificially partitioning classic datasets, e.g., CIFAR-10/100 [78], MNIST [81] or ImageNet [34], on a given number of clients. Common approaches to produce synthetic partitions of classification datasets include associating samples from a limited number of classes to each client [97], Dirichlet sampling on the class labels [59, 133], and using Pachinko Allocation Method (PAM) [84, 110] (which is only possible when the labels have a hierarchical structure). In the case of regression tasks, [105] partitions the *superconduct* dataset [17] across 20 clients using Gaussian Mixture clustering based on T-SNE representations [124] of the features. Such synthetic partition approaches may fall short of modelling the complex statistical heterogeneity of real federated datasets. Evaluating FL strategies on datasets with natural client splits is a safer approach to ensuring that new strategies address real-world issues.

For *cross-device* FL, the LEAF dataset suite [16] includes five datasets with natural partition, spanning a wide range of machine learning tasks: natural language modeling (Reddit [127]), next character prediction (Shakespeare [97]), sentiment analysis (Sent140 [45]), image classification (CelebA [88]) and handwritten-character recognition (FEMNIST [25]). TensorFlow Federated [12] complements LEAF and provides three additional naturally split federated benchmarks, i.e., StackOverflow [120], Google Landmark v2 [60] and iNaturalist [125]. Further, FLSim [111] provides cross-device examples based on LEAF and CIFAR10 [78] with a synthetic split, and FedScale [80] introduces a large FL benchmark focused on mobile applications. Apart from iNaturalist, the aforementioned datasets target the cross-device setting.

To the best of our knowledge, no extensive benchmark with natural splits is available for *cross-silo* FL. However, some standalone works built cross-silo datasets with real partitions. [46] and [95] partition Cityscapes [27] and iNaturalist [125], respectively, exploiting the geolocation of the picture

acquisition site. [58] releases a real-world, geo-tagged dataset of common mammals on Flickr. [92] gathers a federated cross-silo benchmark for object detection created using street cameras. [28] partitions Vehicle Sensor Dataset [38] and Human Activity Recognition dataset [4] by sensor and by individuals, respectively. [93] builds an iris recognition federated dataset across five clients using multiple iris datasets [128, 135, 136, 106]. While FedML [53] introduces several cross-silo benchmarks [54, 132, 52], the related client splits are synthetically obtained with Dirichlet sampling and not based on a natural split. Similarly, FATE [41] provides several cross-silo examples but, to the best of our knowledge, none of them stems from a natural split.

In the medical domain, several works use natural splits replicating the data collection process in different hospitals: the works [2, 18, 8, 72, 130, 19] respectively use the Camelyon datasets [87, 10, 9], the CheXpert dataset [65], LIDC dataset [5], the chest X-ray dataset [76], the IXI dataset [130], the Kaggle diabetic retinopathy detection dataset [47]. Finally, the works [3, 48, 89] use the TCGA dataset [121] by extracting the Tissue Source site metadata.

Our work aims to give more visibility to such isolated cross-silo initiatives by regrouping seven medical datasets, some of which listed above, in a single benchmark suite. We also provide reproducible code alongside precise benchmarking guidelines in order to connect past and subsequent works for a better monitoring of the progress in cross-silo FL.

3 The FLamby Dataset Suite

3.1 Structure Overview

The FLamby datasets suite is a Python library organized in two main parts: datasets with corresponding baseline models, and FL strategies with associated benchmarking code. The suite is modular, with a standardized simple application programming interface (API) for each component, enabling easy re-use and extensions of different components. Further, the suite is compatible with existing FL software libraries, such as FedML [53], Fed-BioMed [117], or Substra [44]. Listing 1 provides a code example of how the structure of FLamby allows to test new datasets and strategies in a few lines of code, and Table 1 provides an overview of the FLamby datasets.

Dataset and baseline model. The FLamby suite contains datasets with a natural notion of client split, as well as a predefined task and associated metric. A train/test set is predefined for each client to enable reproducible comparisons. We further provide a baseline model for each task, with a reference implementation for training on pooled data. For each dataset, the suite provides documentation, metadata and helper functions to: 1. download the original pooled dataset; 2. apply preprocessing if required, making it suitable for ML training; 3. split each original pooled dataset between its natural clients; and 4. easily iterate over the preprocessed dataset. The dataset API relies on PyTorch [102], which makes it easy to iterate over the dataset with natural splits as well as to modify these splits if needed.

FL strategies and benchmark. FL training algorithms, called *strategies* in the FLamby suite, are provided for simulation purposes. In order to be agnostic to existing FL libraries, these strategies are provided in plain Python code. The API of these strategies is standardized and compatible with the dataset API, making it easy to benchmark each strategy on each dataset. We further provide a script performing such a benchmark for illustration purposes. We stress the fact that it is easy to alternatively use implementations from existing FL libraries.

3.2 Datasets, Metrics and Baseline Models

We provide a brief description of each dataset in the FLamby dataset suite, which is summarized in Table 1. In Section 3.4, we further explore the heterogeneity of each dataset, as displayed in Figure 1.

Fed-Camelyon16. Camelyon16 [87] is a histopathology dataset of 399 digitized breast biopsies' slides with or without tumor collected from two hospitals: Radboud University Medical Center (RUMC) and University Medical Center Utrecht (UMCU). By recovering the original split information we build a federated version of Camelyon16 with 2 clients. The task consists in binary classification

of each slide, which is challenging due to the large size of each image ($10^5 \times 10^5$ pixels at 20X magnification), and measured by the Area Under the ROC curve (AUC).

As a baseline, we follow a weakly-supervised learning approach. Slides are first converted to bags of local features, which are one order of magnitude smaller in terms of memory requirements, and a model is then trained on top of this representation. For each slide, we detect regions with a matter-detection network and then extract features from each tile with an ImageNet-pretrained Resnet50, following state-of-the-art practice [29, 90]. Note that due to the imbalanced distribution of tissue in the different slides, a different number of features is produced for each slide: we cap the total number of tiles to 10^5 and use zero-padding for consistency. We then train a DeepMIL architecture [63], using its reference implementation [64] and hyperparameters from [33]. We refer to Appendix C for more details.

Fed-LIDC-IDRI. LIDC-IDRI [5, 62, 23] is an image database [23] study with 1018 CT-scans (3D images) from The Cancer Imaging Archive (TCIA), proposed in the LUNA16 competition [114]. The task consists in automatically segmenting lung nodules in CT-scans, as measured by the DICE score [36]. It is challenging because lung nodules are small, blurry, and hard to detect. By parsing the metadata of the CT-scans from the provided annotations, we recover the manufacturer of each scanning machine used, which we use as a proxy for a client. We therefore build a 4-client federated version of this dataset, split by manufacturer. Figure 1b displays the distribution of voxel intensities in each client.

As a baseline model, we use a VNet [98] following the implementation from [100]. This model is trained by sampling 3D-volumes into 3D patches fitting in GPU memory. Details of the sampling procedure are available in Appendix D.

Fed-IXI. This dataset is extracted from the Information eXtraction from Images - IXI database [35], and has been previously released by Perez *et al.* [108, 104] under the name of *IXITiny*. *IXITiny* provides a database of brain T1 magnetic resonance images (MRIs) from 3 hospitals (Guys, HH, and IOP). This dataset has been adapted to a brain segmentation task by obtaining spatial brain masks using a state-of-the-art unsupervised brain segmentation tool [61]. The quality of the resulting supervised segmentation task is measured by the DICE score [36].

The image pre-processing pipeline includes volume resizing to $48 \times 60 \times 48$ voxels, and sample-wise intensity normalization. Figure 1c highlights the heterogeneity of the raw MRI intensity distributions between clients. As a baseline, we use a 3D U-net [22] following the implementation of [107]. Appendix E provides more detailed information about this dataset, including demographic information, and about the baseline.

Fed-TCGA-BRCA. The Cancer Genome Atlas (TCGA)’s Genomics Data Commons (GDC) portal [99] contains multi-modal data (tabular, 2D and 3D images) on a variety of cancers collected in many different hospitals. Here, we focus on clinical data from the BReast CAncer study (BRCA), which includes features gathered from 1066 patients. We use the Tissue Source Site metadata to split data based on extraction site, grouped into geographic regions to obtain large enough clients. We end up with 6 clients: USA (Northeast, South, Middlewest, West), Canada and Europe, with patient counts varying from 51 to 311. The task consists in predicting survival outcomes [70] based on the patients’ tabular data (39 features overall), with the event to predict being death. This survival task is akin to a ranking problem with the score of each sample being known either directly or only by lower bound (right censorship). The ranking is evaluated by using the concordance index (C-index) that measures the percentage of correctly ranked pairs while taking censorship into account.

As a baseline, we use a linear Cox proportional hazard model [30] to predict time-to-death for patients. Figure 1e highlights the survival distribution heterogeneity between the different clients. Appendix F provides more details on this dataset.

Fed-KITS2019. The KiTS19 dataset [55, 56] stems from the Kidney Tumor Segmentation Challenge 2019 and contains CT scans of 210 patients along with the segmentation masks from 79 hospitals. We recover the hospital metadata and extract a 6-client federated version of this dataset by removing hospitals with less than 10 training samples. The task consists of both kidney and tumor segmentation, labeled 1 and 2, respectively, and we measure the average of Kidney and Tumor DICE scores [36] as our evaluation metric.

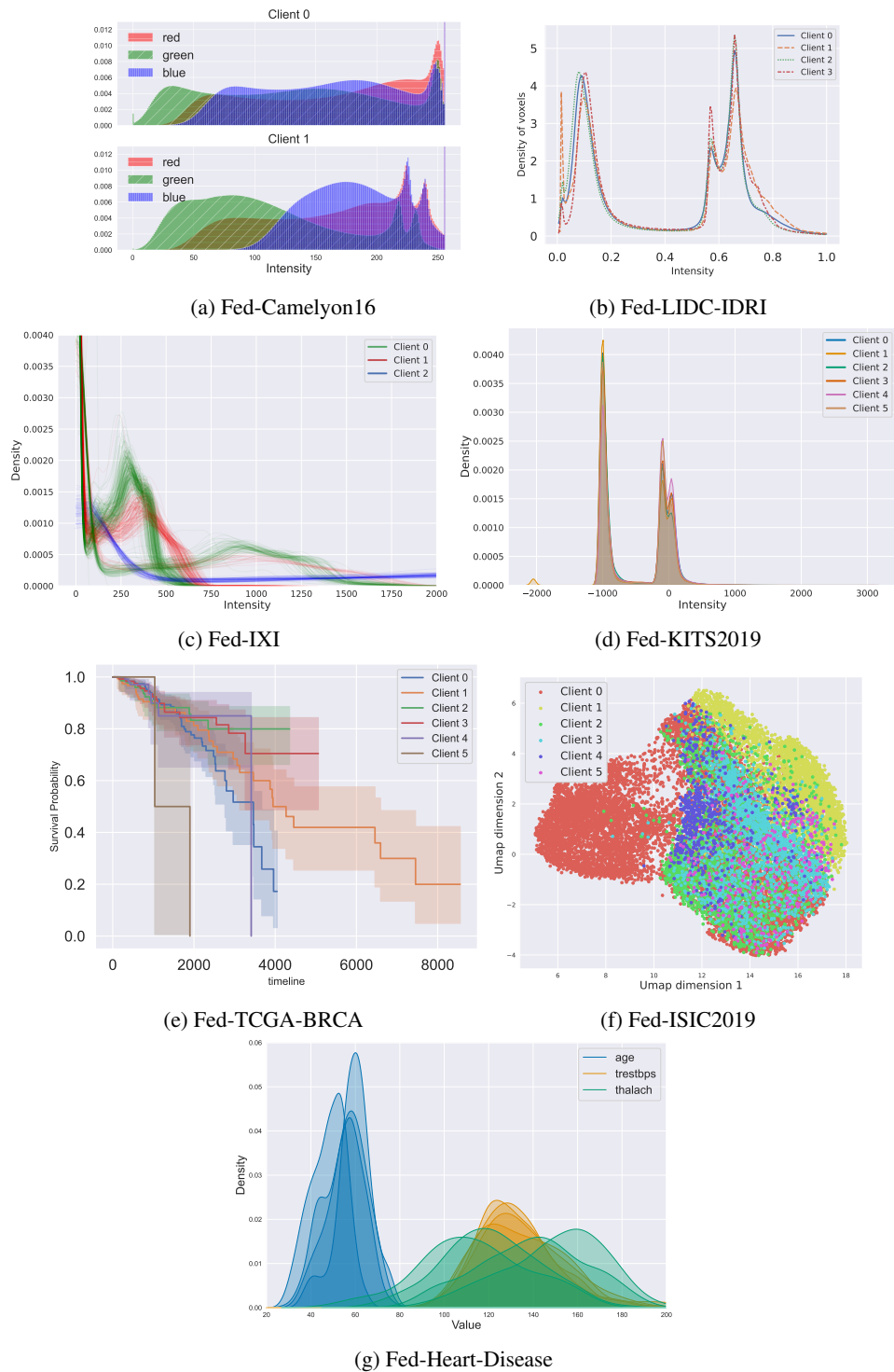


Figure 1: Heterogeneity of FLamby datasets. Best seen in color. 1a: Color histograms per client. 1b, 1c and 1d: Voxel intensity distribution per client. 1e: Kaplan-Meier survival curves per client. 1f: UMAP of deep network features of the raw images, colored by client. 1g: Per-client histograms of several features. Differences between client distributions are sometimes obvious and sometimes subtle. Some clients are close in the feature space, some are not and different types of heterogeneity are observed with different data modalities.

The preprocessing pipeline comprises intensity clipping followed by intensity normalization, and resampling of all the cases to a common voxel spacing of 2.90x1.45x1.45 mm. As a baseline, we use the nn-Unet library [67] to train a 3D nnU-Net, combined with multiple data augmentations including scaling, rotations, brightness, contrast, gamma and Gaussian noise with the batch generators framework [66]. Appendix G provides more details on this dataset.

Fed-ISIC2019. The ISIC2019 dataset [123, 24, 26] contains dermoscopy images collected in 4 hospitals. We restrict ourselves to 23,247 images from the public train set due to metadata availability reasons, which we re-split into train and test sets. The task consists in image classification among 8 different melanoma classes, with high label imbalance (prevalence ranging 49% to less than 1% depending on the class). We split this dataset based on the imaging acquisition system used: as one hospital used 3 different imaging technologies throughout time, we end up with a 6-client federated version of ISIC2019. We measure classification performance through balanced accuracy, defined as the average recall on each class.

As an offline preprocessing step, we follow recommendations and code from [6] by resizing images to the same shorter side while maintaining their aspect ratio, and by normalizing images’ brightness and contrast through a color consistency algorithm. As a baseline classification model, we fine-tune an EfficientNet [119] pretrained on ImageNet, with a weighted focal loss [86] and with multiple data augmentations. Figure 1f highlights the heterogeneity between the different clients prior to preprocessing. Appendix H provides more details on this dataset.

Fed-Heart-Disease. The Heart-Disease dataset [68] was collected in 4 hospitals in the USA, Switzerland and Hungary. This dataset contains tabular information about 740 patients distributed among these four clients. The task consists in binary classification to assess the presence or absence of heart disease. We preprocess the dataset by removing missing values and encoding non-binary categorical variables as dummy variables, which gives 13 relevant attributes. As a baseline model, we use logistic regression. Appendix I provides more details on this dataset.

3.3 Federated Learning Strategies in FLamby

The following standard FL algorithms, called *strategies*, are implemented in FLamby. We rely on a common API for all strategies, which allows for efficient benchmarking of both datasets and strategies, as shown in Listing 1. As we focus on the cross-silo setting, we restrict ourselves to strategies with full client participation.

FedAvg [97]. FedAvg is the simplest FL strategy. It performs iterative round-based training, each round consisting in local mini-batch updates on each client followed by parameter averaging on a central server. As a convention, we choose to count the number of local updates in batches and not in local epochs in order to match theoretical formulations of this algorithm; this choice also applies to strategies derived from FedAvg. This strategy is known to be sensitive to heterogeneity when the number of local updates grows [83, 75].

FedProx [83]. In order to mitigate statistical heterogeneity, FedProx builds on FedAvg by introducing a regularization term to each local training loss, thereby controlling the deviation of the local models from the last global model.

Scaffold [75]. Scaffold mitigates client drifts using control-variates and by adding a server-side learning rate. We implement a full-participation version of Scaffold that is optimized to reduce the number of bits communicated between the clients and the server.

Cyclic Learning [19, 116]. Cyclic Learning performs local optimizations on each client in a sequential fashion, transferring the trained model to the next client when training finishes. Cyclic is a simple sequential baseline to other federated strategies. For Cyclic, we define a round as a full cycle throughout all clients. We implement both such cycles in a fixed order or in a shuffled order at each round.

FedAdam [110], FedYogi [110], FedAdagrad [110]. FedAdam, FedYogi and FedAdagrad are generalizations of their respective single-centric optimizers (Adam [77], Yogi [134] and Adagrad [94]) to the FL setting. In all cases, the running means and variances of the updates are tracked at the server level.

```

# Import relevant dataset, strategy, and utilities
from flamby.datasets.fed_camelyon16 import FedCamelyon16, Baseline, BaselineLoss, NUM_CLIENTS, metric
from flamby.strategies import FedProx
from flamby.utils import evaluate_model_on_tests, get_nb_max_rounds

# Define number of local updates and number of rounds
num_updates = 100
num_rounds = get_nb_max_rounds(num_updates)
# Dataloaders for train and test
training_dataloaders = [
    DataLoader(FedCamelyon16(center=i, train=True, pooled=False), batch_size=BATCH_SIZE, shuffle=True)
    for i in range(NUM_CLIENTS)
]
test_dataloaders = [
    DataLoader(FedCamelyon16(center=i, train=False, pooled=False), batch_size=BATCH_SIZE, shuffle=False)
    for i in range(NUM_CLIENTS)
]
# Define local model and loss
model_baseline = Baseline()
loss_baseline = BaselineLoss()
# Define and train strategy
strategy = FedProx(training_dataloaders, model_baseline, loss_baseline, torch.optim.SGD, LR, num_updates, num_rounds)
model_final = strategy.run()[0]
# Evaluate final FL model on test sets
results_per_client = evaluate_model_on_tests(model_final, test_dataloaders, metric)

```

Listing 1: Code example from the FLamby dataset suite: on the Fed-Camelyon16 dataset, we use the FedProx Federated Learning strategy to train the pre-implemented baseline model.

3.4 Dataset Heterogeneity

We qualitatively illustrate the heterogeneity of the datasets of FLamby. For each dataset, we compute a relevant statistical distribution for each client, which differs due to the differences in tasks and modalities of the datasets. We comment the results displayed in Figure 1 in the following. Appendix M provides a more quantitative exploration of this heterogeneity.

For the **Fed-Camelyon16** dataset, we display the color histograms (RGB values) of the raw tissue patches in each client. We see that the RGB distributions of both clients strongly differ. For both **Fed-LIDC-IDRI** and **Fed-KITS2019** datasets, we display histograms of voxel intensities. In both cases, we do not note significant differences between clients. For the **Fed-IXI** dataset, we display the histograms of raw T1-MRI images, showing visible differences between clients. For **Fed-TCGA-BRCA**, we display Kaplan-Meier estimations of the survival curves [73] in each client. As detailed in Appendix F, pairwise log-rank tests demonstrate significant differences between some clients, but not all. For the **Fed-ISIC2019**, we use a 2-dimensional UMAP [96] plot of the features extracted from an Imagenet-pretrained Efficientnetv1 on the raw images. We see that some clients are isolated in distinct clusters, while others overlap, highlighting the heterogeneity of this dataset. Last, for the **Fed-Heart-Disease** dataset, we display histograms for a subset of features (age, resting blood pressure and maximum heart rate), showing that feature distributions vary between clients.

4 FL Benchmark Example with FLamby

In this section, we detail the guidelines we follow to perform a benchmark and provide results thereof. These guidelines might be used in the future to facilitate fair comparisons between potentially novel FL strategies and existing ones. However, we stress that FLamby also allows for any other experimental setup thanks to its modular structure, as we showcase in Appendices L.1 and L.2. The FLamby suite further provides a script to automatically reproduce this benchmark based on configuration files.

Train/test split. We use the per-client train/test splits, including all clients for training. Performance is evaluated on each local test dataset, and then averaged across the clients. We exclude model personalization from this benchmark: therefore, a single model is evaluated at the end of training. We refer to Appendix L.2 for more results with model personalization.

Hyperparameter tuning and Baselines. We distinguish two kinds of hyperparameters: those related to the machine learning (ML) part itself, and those related to the FL strategy. We tune these parameters separately, starting with the machine learning part. All experiments are repeated with 5 independent runs, except for FED-LIDC-IDRI where only 1 training is performed due to a long training time.

For each dataset, the ML hyperparameters include the model architecture, the loss and related hyperparameters, including local batch size. These ML hyperparameters are carefully tuned with cross-validation on the pooled training data. The resulting ML model gives rise to the **pooled baseline**. We use the same ML hyperparameters for training on each client individually, leading to **local baselines**.

For the FL strategies, hyperparameters include e.g. local learning rate, server learning rate, and other relevant quantities depending on the strategies. For each dataset and each FL strategy, we use the same model as in the pooled and local baselines, with fixed hyperparameters. We then only optimize FL strategies-related hyperparameters.

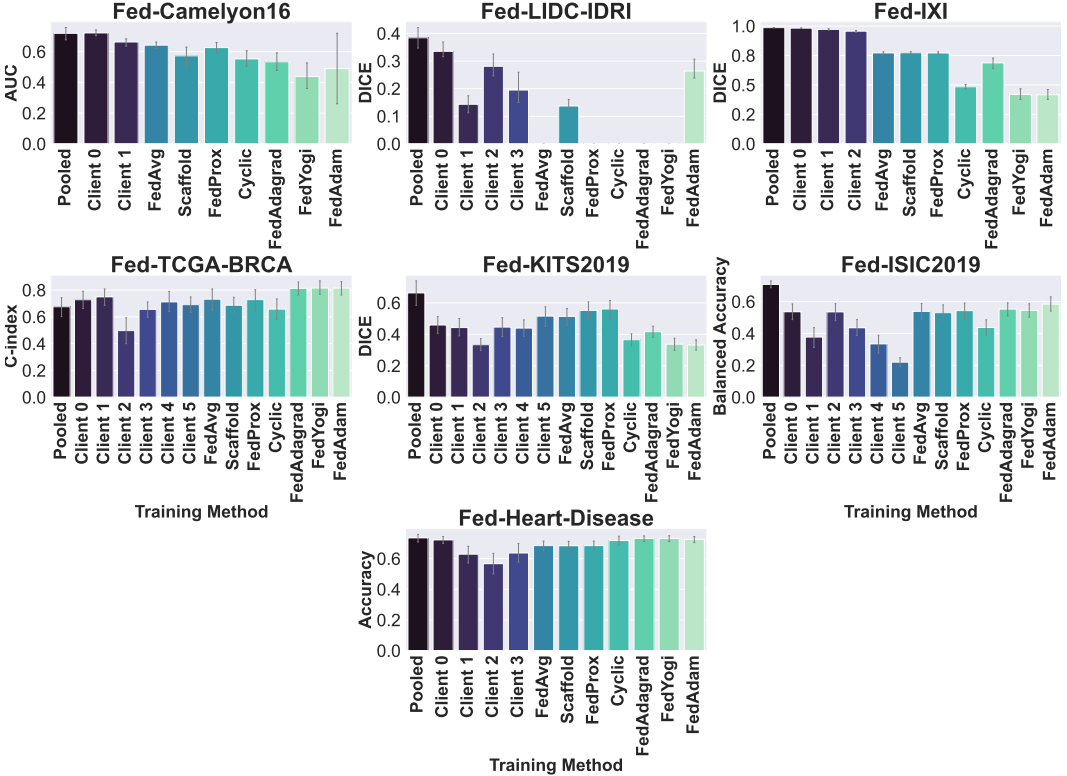


Figure 2: Benchmark results on FLamby for each dataset. For all metrics, higher is better, see Section 3.2 for metric details and Section 4 for experimental details. For Fed-LIDC-IDRI, multiple strategies fail converging, leading to zero DICE. Except for Fed-TCGA-BRCA and Fed-Heart-Disease, federated strategies fall short of reaching the pooled performance, but improve over the local ones.

Federated setup. For all strategies and datasets, the number of rounds T_{\max} is fixed to perform approximately as many epochs on each client as is necessary to get good performance when data is pooled. Note that, as we use a single batch size B and a fixed number E of local steps, the notion of epoch is ill-defined; we approximate it as follows. Given n_{epochs}^P , the number of epochs required to train the baseline model for the pooled dataset, n_T the total number of samples in the distributed training set, K the number of clients, we define

$$T_{\max} = n_{epochs}^P \cdot \lfloor n_T / K / B / E \rfloor \quad (1)$$

where $\lfloor \cdot \rfloor$ denotes the floor operation. In our benchmark, we use $E = 100$ local updates for all datasets. Note that this restriction in the total number of rounds may have an impact on the convergence of federated strategies. We refer to Appendix J for more details on this benchmark.

Benchmark results. The test results of the benchmark are displayed in Figure 2. Note that test results are uniformly averaged over the different local clients. We observe strikingly different behaviours across datasets.

No local training or FL strategy is able to reach a performance on par with the pooled training, except for Fed-TCGA-BRCA and Fed-Heart-Disease. It is remarkable that both of them are tabular, low-dimensional datasets, with only linear models. Still, for Fed-KITS2019 and Fed-ISIC2019, some FL strategies outperform local training, showing the benefit of collaboration, but falling short of reaching pooled performance. For Fed-Camelyon16, Fed-LIDC-IDRI and Fed-IXI, the current results do not indicate any benefit in collaborative training.

Among FL strategies, we note that for the datasets where an FL strategy outperforms the pooled baselines, FedOpt variants (FedAdagrad, FedYogi and FedAdam) reach the best performance. Further, the Cyclic baseline systematically underperforms other strategies. Last, but not least, FedAvg does not reach top performance among FL strategies, except for Fed-Camelyon16 and Fed-IXI, it remains a competitive baseline strategy.

These results show the difficulty of tuning properly FL strategies, especially in the case of heterogeneous cross-silo datasets. This calls for the development of more robust FL strategies in this setting.

5 Conclusion

In this article we introduce FLamby, a modular dataset suite and benchmark, comprising multiple tasks and data modalities, and reflecting the heterogeneity of real-world healthcare cross-silo FL use cases. This comprehensive benchmark is needed to advance the understanding of cross-silo healthcare data collection on FL performance.

Currently, FLamby is limited to healthcare datasets. In the longer run and with the help of the FL community, it could be enriched with datasets from other application domains to better reflect the diversity of cross-silo FL applications, which is possible thanks to its modular design. Regarding machine learning backends, FLamby only provides PyTorch [102] code: supporting other backends, such as TensorFlow [1] or JAX [14], is a relevant future direction if there is such demand from the community. Further, our benchmark currently does not integrate all constraints of cross-silo FL, especially privacy aspects, which are important in this setting.

In terms of FL setting, the benchmark mainly focuses on the heterogeneity induced by natural splits. In order to make it more realistic, future developments might include in depth study of Differential Privacy (DP) training [39], cryptographic protocols such as Secure Aggregation [13], Personalized FL [40], or communication constraints [113] when applicable. As we showcase in Appendices L.1 for DP and L.2 for personalization, the structure of FLamby makes it possible to quickly tackle such questions. We hope that the scientific community will use FLamby for cross-silo research purposes on real data, and contribute to further develop it, making it a reference for this research topic.

Acknowledgments and Disclosure of Funding

The authors thank the anonymous reviewers, ethics reviewer, and meta-reviewer for their feedback and ideas, which significantly improved the paper and the repository. The authors listed as Owkin, Inc. employees are supported by Owkin, Inc. The works of E.M. and S.A. is supported, in part, by gifts from Intel and Konica Minolta. This work was supported by the Swiss State Secretariat for Education, Research and Innovation (SERI) under contract number 22.00133, by the Inria Explorator Action FLAMED and by the French National Research Agency (grant ANR-20-CE23-0015, project PRIDE and ANR-20-THIA-0014 program AI_PhD@Lille). This project has also received funding from the European Union’s Horizon 2020 research and innovation programme under grant agreement No 847581 and is co-funded by the Region Provence-Alpes-Côte d’Azur and IDEX UCAJEDI. A.D.’s research was supported by the *Statistics and Computation for AI* ANR Chair and by *Hi!Paris*. C.P. received support from *Accenture Labs* (Sophia Antipolis, France).

References

- [1] Martín Abadi, Ashish Agarwal, Paul Barham, Eugene Brevdo, Zhifeng Chen, Craig Citro, Greg S. Corrado, Andy Davis, Jeffrey Dean, Matthieu Devin, Sanjay Ghemawat, Ian Goodfellow, Andrew Harp, Geoffrey Irving, Michael Isard, Yangqing Jia, Rafal Jozefowicz, Lukasz Kaiser, Manjunath Kudlur, Josh Levenberg, Dandelion Mané, Rajat Monga, Sherry Moore, Derek Murray, Chris Olah, Mike Schuster, Jonathon Shlens, Benoit Steiner, Ilya Sutskever, Kunal Talwar, Paul Tucker, Vincent Vanhoucke, Vijay Vasudevan, Fernanda Viégas, Oriol Vinyals, Pete Warden, Martin Wattenberg, Martin Wicke, Yuan Yu, and Xiaoqiang Zheng. TensorFlow: Large-scale machine learning on heterogeneous systems, 2015. Software available from tensorflow.org.
- [2] Mathieu Andreux, Jean Ogier du Terrail, Constance Beguier, and Eric W Tramel. Siloed federated learning for multi-centric histopathology datasets. In *Domain Adaptation and Representation Transfer, and Distributed and Collaborative Learning*, pages 129–139. Springer, 2020.
- [3] Mathieu Andreux, Andre Manoel, Romuald Menuet, Charlie Saillard, and Chloé Simpson. Federated survival analysis with discrete-time Cox models. *arXiv preprint arXiv:2006.08997*, 2020.
- [4] Davide Anguita, Alessandro Ghio, Luca Oneto, Xavier Parra Perez, and Jorge Luis Reyes Ortiz. A public domain dataset for human activity recognition using smartphones. In *Proceedings of the 21th international European symposium on artificial neural networks, computational intelligence and machine learning*, pages 437–442, 2013.
- [5] Samuel G Armato III, Geoffrey McLennan, Luc Bidaut, Michael F McNitt-Gray, Charles R Meyer, Anthony P Reeves, Binsheng Zhao, Denise R Aberle, Claudia I Henschke, Eric A Hoffman, et al. The lung image database consortium (LIDC) and image database resource initiative (IDRI): a completed reference database of lung nodules on ct scans. *Medical physics*, 38(2):915–931, 2011.
- [6] Aman Arora. Siim-istic melanoma classification - my journey to a top 5% solution and first silver medal on kaggle. <https://amaarora.github.io/2020/08/23/siimistic.html>. Accessed: 2022-02-02.
- [7] Aldo Badano, Craig Revie, Andrew Casertano, Wei-Chung Cheng, Phil Green, Tom Kimpe, Elizabeth Krupinski, Christye Sisson, Stein Skrøvseth, Darren Treanor, et al. Consistency and standardization of color in medical imaging: a consensus report. *Journal of digital imaging*, 28(1):41–52, 2015.
- [8] Pragati Baheti, Mukul Sikka, KV Arya, and R Rajesh. Federated learning on distributed medical records for detection of lung nodules. In *VISIGRAPP (4: VISAPP)*, pages 445–451, 2020.
- [9] Peter Bandi, Oscar Geessink, Quirine Manson, Marcory Van Dijk, Maschenka Balkenhol, Meyke Hermsen, Babak Ehteshami Bejnordi, Byungjae Lee, Kyunghyun Paeng, Aoxiao Zhong, et al. From detection of individual metastases to classification of lymph node status at the patient level: the camelyon17 challenge. *IEEE transactions on medical imaging*, 38(2):550–560, 2018.
- [10] Babak Ehteshami Bejnordi, Mitko Veta, Paul Johannes Van Diest, Bram Van Ginneken, Nico Karssemeijer, Geert Litjens, Jeroen AWM Van Der Laak, Meyke Hermsen, Quirine F Manson, Maschenka Balkenhol, et al. Diagnostic assessment of deep learning algorithms for detection of lymph node metastases in women with breast cancer. *Jama*, 318(22):2199–2210, 2017.
- [11] Abhishek Bhowmick, John Duchi, Julien Freudiger, Gaurav Kapoor, and Ryan Rogers. Protection against reconstruction and its applications in private federated learning. *arXiv preprint arXiv:1812.00984*, 2018.
- [12] Keith Bonawitz, Hubert Eichner, Wolfgang Grieskamp, Dzmitry Huba, Alex Ingerman, Vladimir Ivanov, Chloe Kiddon, Jakub Konečný, Stefano Mazzocchi, Brendan McMahan, et al. Towards federated learning at scale: System design. *Proceedings of Machine Learning and Systems*, 1:374–388, 2019.

- [13] Keith Bonawitz, Vladimir Ivanov, Ben Kreuter, Antonio Marcedone, H Brendan McMahan, Sarvar Patel, Daniel Ramage, Aaron Segal, and Karn Seth. Practical secure aggregation for privacy-preserving machine learning. In *proceedings of the 2017 ACM SIGSAC Conference on Computer and Communications Security*, pages 1175–1191, 2017.
- [14] James Bradbury, Roy Frostig, Peter Hawkins, Matthew James Johnson, Chris Leary, Dougal Maclaurin, George Necula, Adam Paszke, Jake VanderPlas, Skye Wanderman-Milne, and Qiao Zhang. JAX: composable transformations of Python+NumPy programs, 2018.
- [15] Talha Burki. Pharma blockchains AI for drug development. *The Lancet*, 393(10189):2382, 2019.
- [16] Sebastian Caldas, Sai Meher Karthik Duddu, Peter Wu, Tian Li, Jakub Konečný, H Brendan McMahan, Virginia Smith, and Ameet Talwalkar. Leaf: A benchmark for federated settings. *arXiv preprint arXiv:1812.01097*, 2018.
- [17] Rich Caruana, Thorsten Joachims, and Lars Backstrom. KDD-Cup 2004: results and analysis. *ACM SIGKDD Explorations Newsletter*, 6(2):95–108, 2004.
- [18] Arunava Chakravarty, Avik Kar, Ramanathan Sethuraman, and Debdoot Sheet. Federated learning for site aware chest radiograph screening. In *2021 IEEE 18th International Symposium on Biomedical Imaging (ISBI)*, pages 1077–1081. IEEE, 2021.
- [19] Ken Chang, Niranjana Balachandar, Carson Lam, Darwin Yi, James Brown, Andrew Beers, Bruce Rosen, Daniel L Rubin, and Jayashree Kalpathy-Cramer. Distributed deep learning networks among institutions for medical imaging. *Journal of the American Medical Informatics Association*, 25(8):945–954, 2018.
- [20] Zachary Charles, Zachary Garrett, Zhouyuan Huo, Sergei Shmulyian, and Virginia Smith. On large-cohort training for federated learning. *arXiv preprint arXiv:2106.07820*, 2021.
- [21] Aakanksha Chowdhery, Sharan Narang, Jacob Devlin, Maarten Bosma, Gaurav Mishra, Adam Roberts, Paul Barham, Hyung Won Chung, Charles Sutton, Sebastian Gehrmann, et al. Palm: Scaling language modeling with pathways. *arXiv preprint arXiv:2204.02311*, 2022.
- [22] Özgün Çiçek, Ahmed Abdulkadir, Soeren S Lienkamp, Thomas Brox, and Olaf Ronneberger. 3d u-net: learning dense volumetric segmentation from sparse annotation. In *International conference on medical image computing and computer-assisted intervention*, pages 424–432. Springer, 2016.
- [23] Kenneth Clark, Bruce Vendt, Kirk Smith, John Freymann, Justin Kirby, Paul Koppel, Stephen Moore, Stanley Phillips, David Maffitt, Michael Pringle, et al. The cancer imaging archive (TCIA): maintaining and operating a public information repository. *Journal of digital imaging*, 26(6):1045–1057, 2013.
- [24] Noel CF Codella, David Gutman, M Emre Celebi, Brian Helba, Michael A Marchetti, Stephen W Dusza, Aadi Kalloo, Konstantinos Liopyris, Nabin Mishra, Harald Kittler, et al. Skin lesion analysis toward melanoma detection: A challenge at the 2017 international symposium on biomedical imaging (ISBI), hosted by the international skin imaging collaboration (ISIC). In *2018 IEEE 15th international symposium on biomedical imaging (ISBI 2018)*, pages 168–172. IEEE, 2018.
- [25] Gregory Cohen, Saeed Afshar, Jonathan Tapson, and Andre Van Schaik. EMNIST: Extending MNIST to handwritten letters. In *2017 International Joint Conference on Neural Networks (IJCNN)*, pages 2921–2926. IEEE, 2017.
- [26] Marc Combalia, Noel CF Codella, Veronica Rotemberg, Brian Helba, Veronica Vilaplana, Ofer Reiter, Cristina Carrera, Alicia Barreiro, Allan C Halpern, Susana Puig, et al. Bcn20000: Dermoscopic lesions in the wild. *arXiv preprint arXiv:1908.02288*, 2019.
- [27] Marius Cordts, Mohamed Omran, Sebastian Ramos, Timo Rehfeld, Markus Enzweiler, Rodrigo Benenson, Uwe Franke, Stefan Roth, and Bernt Schiele. The cityscapes dataset for semantic urban scene understanding. In *Proc. of the IEEE Conference on Computer Vision and Pattern Recognition (CVPR)*, 2016.

- [28] Luca Corinzia, Ami Beuret, and Joachim M Buhmann. Variational federated multi-task learning. *arXiv preprint arXiv:1906.06268*, 2019.
- [29] Pierre Courtiol, Eric W Tramel, Marc Sanselme, and Gilles Wainrib. Classification and disease localization in histopathology using only global labels: A weakly-supervised approach. *arXiv preprint arXiv:1802.02212*, 2018.
- [30] David R Cox. Regression models and life-tables. *Journal of the Royal Statistical Society: Series B (Methodological)*, 34(2):187–202, 1972.
- [31] Ittai Dayan, Holger R Roth, Aoxiao Zhong, Ahmed Harouni, Amilcare Gentili, Anas Z Abidin, Andrew Liu, Anthony Beardsworth Costa, Bradford J Wood, Chien-Sung Tsai, et al. Federated learning for predicting clinical outcomes in patients with covid-19. *Nature medicine*, 27(10):1735–1743, 2021.
- [32] Kevin de Haan, Yijie Zhang, Jonathan E Zuckerman, Tairan Liu, Anthony E Sisk, Miguel FP Diaz, Kuang-Yu Jen, Alexander Nobori, Sofia Liou, Sarah Zhang, et al. Deep learning-based transformation of H&E stained tissues into special stains. *Nature communications*, 12(1):1–13, 2021.
- [33] Olivier Dehaene, Axel Camara, Olivier Moindrot, Axel de Lavergne, and Pierre Courtiol. Self-supervision closes the gap between weak and strong supervision in histology. *arXiv preprint arXiv:2012.03583*, 2020.
- [34] Jia Deng, Wei Dong, Richard Socher, Li-Jia Li, Kai Li, and Li Fei-Fei. Imagenet: A large-scale hierarchical image database. In *2009 IEEE conference on computer vision and pattern recognition*, pages 248–255. Ieee, 2009.
- [35] Brain development team. Ixi dataset. <https://brain-development.org/ixi-dataset/>. Accessed: 2022-02-02.
- [36] Lee R Dice. Measures of the amount of ecologic association between species. *Ecology*, 26(3):297–302, 1945.
- [37] Jean Ogier du Terrail, Armand Leopold, Clément Joly, Constance Beguier, Mathieu Andreux, Charles Maussion, Benoit Schmauch, Eric W Tramel, Etienne Bendjebbar, Mikhail Zaslavskiy, et al. Collaborative federated learning behind hospitals’ firewalls for predicting histological response to neoadjuvant chemotherapy in triple-negative breast cancer. *medRxiv*, 2021.
- [38] Marco F Duarte and Yu Hen Hu. Vehicle classification in distributed sensor networks. *Journal of Parallel and Distributed Computing*, 64(7):826–838, 2004.
- [39] Cynthia Dwork, Aaron Roth, et al. The algorithmic foundations of differential privacy. *Found. Trends Theor. Comput. Sci.*, 9(3-4):211–407, 2014.
- [40] Alireza Fallah, Aryan Mokhtari, and Asuman Ozdaglar. Personalized federated learning: A meta-learning approach. *arXiv preprint arXiv:2002.07948*, 2020.
- [41] FedAI-maintainers. Fate (federated ai technology enabler). <https://github.com/FederatedAI/FATE>. Accessed: 2022-10-12.
- [42] Yann Fraboni, Richard Vidal, Laetitia Kameni, and Marco Lorenzi. On the impact of client sampling on federated learning convergence. *arXiv preprint arXiv:2107.12211*, 2021.
- [43] Yu Fu, Alexander W Jung, Ramon Viñas Torne, Santiago Gonzalez, Harald Vöhringer, Artem Shmatko, Lucy R Yates, Mercedes Jimenez-Linan, Luiza Moore, and Moritz Gerstung. Pan-cancer computational histopathology reveals mutations, tumor composition and prognosis. *Nature Cancer*, 1(8):800–810, 2020.
- [44] Mathieu N Galtier and Camille Marini. Substra: a framework for privacy-preserving, traceable and collaborative machine learning. *arXiv preprint arXiv:1910.11567*, 2019.
- [45] Alec Go, Richa Bhayani, and Lei Huang. Twitter sentiment classification using distant supervision. *CS224N project report, Stanford*, 1(12):2009, 2009.

- [46] Xuan Gong, Abhishek Sharma, Srikrishna Karanam, Ziyang Wu, Terrence Chen, David Doremann, and Arun Innanje. Ensemble attention distillation for privacy-preserving federated learning. In *Proceedings of the IEEE/CVF International Conference on Computer Vision*, pages 15076–15086, 2021.
- [47] Ben Graham. Kaggle diabetic retinopathy detection competition report. *University of Warwick*, pages 24–26, 2015.
- [48] Gozde N Gunesli, Mohsin Bilal, Shan E Ahmed Raza, and Nasir M Rajpoot. Feddropoutavg: Generalizable federated learning for histopathology image classification. *arXiv preprint arXiv:2111.13230*, 2021.
- [49] Farzin Haddadpour, Mohammad Mahdi Kamani, Aryan Mokhtari, and Mehrdad Mahdavi. Federated learning with compression: Unified analysis and sharp guarantees. In *International Conference on Artificial Intelligence and Statistics*, pages 2350–2358. PMLR, 2021.
- [50] Peter F Hahn, Michael A Blake, and Giles WL Boland. Adrenal lesions: attenuation measurement differences between ct scanners. *Radiology*, 240(2):458–463, 2006.
- [51] Chaoyang He, Murali Annavam, and Salman Avestimehr. Group knowledge transfer: Federated learning of large CNNs at the edge. *arXiv preprint arXiv:2007.14513*, 2020.
- [52] Chaoyang He, Keshav Balasubramanian, Emir Ceyani, Carl Yang, Han Xie, Lichao Sun, Lifang He, Liangwei Yang, Philip S Yu, Yu Rong, et al. Fedgraphnn: A federated learning system and benchmark for graph neural networks. *arXiv preprint arXiv:2104.07145*, 2021.
- [53] Chaoyang He, Songze Li, Jinhyun So, Xiao Zeng, Mi Zhang, Hongyi Wang, Xiaoyang Wang, Praneeth Vepakomma, Abhishek Singh, Hang Qiu, et al. Fedml: A research library and benchmark for federated machine learning. *arXiv preprint arXiv:2007.13518*, 2020.
- [54] Chaoyang He, Alay Dilipbhai Shah, Zhenheng Tang, Di Fan, Adarshan Naiynar Sivashunmugam, Keerti Bhogaraju, Mita Shimpi, Li Shen, Xiaowen Chu, Mahdi Soltanolkotabi, and Salman Avestimehr. Fedcv: A federated learning framework for diverse computer vision tasks. *arXiv preprint arXiv:2111.11066*, 2021.
- [55] Nicholas Heller, Fabian Isensee, Klaus H Maier-Hein, Xiaoshuai Hou, Chunmei Xie, Fengyi Li, Yang Nan, Guangrui Mu, Zhiyong Lin, Miofei Han, et al. The state of the art in kidney and kidney tumor segmentation in contrast-enhanced ct imaging: Results of the kits19 challenge. *Medical Image Analysis*, page 101821, 2020.
- [56] Nicholas Heller, Niranjana Sathianathan, Arveen Kalapara, Edward Walczak, Keenan Moore, Heather Kaluzniak, Joel Rosenberg, Paul Blake, Zachary Rengel, Makinna Oestreich, et al. The kits19 challenge data: 300 kidney tumor cases with clinical context, ct semantic segmentations, and surgical outcomes. *arXiv preprint arXiv:1904.00445*, 2019.
- [57] Frederick M Howard, James Dolezal, Sara Kochanny, Jeffrey Schulte, Heather Chen, Lara Heij, Dezheng Huo, Rita Nanda, Olufunmilayo I Olopade, Jakob N Kather, et al. The impact of site-specific digital histology signatures on deep learning model accuracy and bias. *Nature communications*, 12(1):1–13, 2021.
- [58] Kevin Hsieh, Amar Phanishayee, Onur Mutlu, and Phillip Gibbons. The non-IID data quagmire of decentralized machine learning. In *International Conference on Machine Learning (ICML)*, pages 5819–5830. PMLR, 2020.
- [59] Tzu-Ming Harry Hsu, Hang Qi, and Matthew Brown. Measuring the effects of non-identical data distribution for federated visual classification. *arXiv preprint arXiv:1909.06335*, 2019.
- [60] Tzu-Ming Harry Hsu, Hang Qi, and Matthew Brown. Federated visual classification with real-world data distribution. In *European Conference on Computer Vision*, pages 76–92. Springer, 2020.
- [61] Juan Eugenio Iglesias, Cheng-Yi Liu, Paul M Thompson, and Zhuowen Tu. Robust brain extraction across datasets and comparison with publicly available methods. *IEEE transactions on medical imaging*, 30(9):1617–1634, 2011.

- [62] S. G. Armato III, G. McLennan, L. Bidaut, M. F. McNitt-Gray, C. R. Meyer, A. P. Reeves, B. Zhao, D. R. Aberle, C. I. Henschke, E. A. Hoffman, E. A. Kazerooni, H. MacMahon, E. J. R. Van Beek, D. Yankelevitz, A. M. Biancardi, P. H. Bland, M. S. Brown, R. M. Engelmann, G. E. Laderach, D. Max, R. C. Pais, D. P. Y. Qing, R. Y. Roberts, A. R. Smith, A. Starkey, P. Batra, P. Caligiuri, A. Farooqi, G. W. Gladish, C. M. Jude, R. F. Munden, I. Petkowska, L. E. Quint, L. H. Schwartz, B. Sundaram, L. E. Dodd, C. Fenimore, D. Gur, N. Petrick, J. Freymann, J. Kirby, B. Hughes, A. V. Castele, S. Gupte and M. Sallam, M. D. Heath, M. H. Kuhn, E. Dharaiya, R. Burns, D. S. Fryd, M. Salganicoff, V. Anand, U. Shreter, S. Vastagh, B. Y. Croft, and L. P. Clarke. Data from lidc-idri [data set]. the cancer imaging archive., 2015.
- [63] Maximilian Ilse, Jakub Tomczak, and Max Welling. Attention-based deep multiple instance learning. In *International conference on machine learning*, pages 2127–2136. PMLR, 2018.
- [64] Maximilian Ilse, Jakub M. Tomczak, and Max Welling. Attention-based deep multiple instance learning. <https://github.com/AMLab-Amsterdam/AttentionDeepMIL>. Accessed: 2022-02-02.
- [65] Jeremy Irvin, Pranav Rajpurkar, Michael Ko, Yifan Yu, Silvana Ciurea-Ilcus, Chris Chute, Henrik Marklund, Behzad Haghgoo, Robyn Ball, Katie Shpanskaya, et al. Chexpert: A large chest radiograph dataset with uncertainty labels and expert comparison. In *Proceedings of the AAAI conference on artificial intelligence*, volume 33, pages 590–597, 2019.
- [66] F Isensee, P Jäger, J Wasserthal, D Zimmerer, J Petersen, S Kohl, J Schock, A Klein, T RoSS, S Wirkert, et al. batchgenerators—a python framework for data augmentation. *Zenodo* <https://doi.org/10.5281/zenodo.3632567>, 2020.
- [67] Fabian Isensee, Paul F Jaeger, Simon AA Kohl, Jens Petersen, and Klaus H Maier-Hein. nnu-net: a self-configuring method for deep learning-based biomedical image segmentation. *Nature methods*, 18(2):203–211, 2021.
- [68] Andras Janosi, William Steinbrunn, Matthias Pfisterer, and Robert Detrano. Heart disease data set, 1988.
- [69] Andrew Janowczyk, Ren Zuo, Hannah Gilmore, Michael Feldman, and Anant Madabhushi. Histoqc: an open-source quality control tool for digital pathology slides. *JCO clinical cancer informatics*, 3:1–7, 2019.
- [70] Stephen P Jenkins. Survival analysis. *Unpublished manuscript, Institute for Social and Economic Research, University of Essex, Colchester, UK*, 42:54–56, 2005.
- [71] Peter Kairouz, H. Brendan McMahan, Brendan Avent, Aurélien Bellet, Mehdi Bennis, Arjun Nitin Bhagoji, Kallista Bonawitz, Zachary Charles, Graham Cormode, Rachel Cummings, Rafael G. L. D’Oliveira, Hubert Eichner, Salim El Rouayheb, David Evans, Josh Gardner, Zachary Garrett, Adrià Gascón, Badih Ghazi, Phillip B. Gibbons, Marco Gruteser, Zaid Harchaoui, Chaoyang He, Lie He, Zhouyuan Huo, Ben Hutchinson, Justin Hsu, Martin Jaggi, Tara Javidi, Gauri Joshi, Mikhail Khodak, Jakub Konecný, Aleksandra Korolova, Farinaz Koushanfar, Sanmi Koyejo, Tancrede Lepoint, Yang Liu, Prateek Mittal, Mehryar Mohri, Richard Nock, Ayfer Özgür, Rasmus Pagh, Hang Qi, Daniel Ramage, Ramesh Raskar, Mariana Raykova, Dawn Song, Weikang Song, Sebastian U. Stich, Ziteng Sun, Ananda Theertha Suresh, Florian Tramèr, Praneeth Vepakomma, Jianyu Wang, Li Xiong, Zheng Xu, Qiang Yang, Felix X. Yu, Han Yu, and Sen Zhao. Advances and open problems in federated learning. *Foundations and Trends® in Machine Learning*, 14(1–2):1–210, 2021.
- [72] Georgios Kaissis, Alexander Ziller, Jonathan Passerat-Palmbach, Théo Ryffel, Dmitrii Usynin, Andrew Trask, Ionésio Lima, Jason Mancuso, Friederike Jungmann, Marc-Matthias Steinborn, et al. End-to-end privacy preserving deep learning on multi-institutional medical imaging. *Nature Machine Intelligence*, 3(6):473–484, 2021.
- [73] Edward L Kaplan and Paul Meier. Nonparametric estimation from incomplete observations. *Journal of the American statistical association*, 53(282):457–481, 1958.
- [74] Jared Kaplan, Sam McCandlish, Tom Henighan, Tom B Brown, Benjamin Chess, Rewon Child, Scott Gray, Alec Radford, Jeffrey Wu, and Dario Amodei. Scaling laws for neural language models. *arXiv preprint arXiv:2001.08361*, 2020.

- [75] Sai Praneeth Karimireddy, Satyen Kale, Mehryar Mohri, Sashank Reddi, Sebastian Stich, and Ananda Theertha Suresh. Scaffold: Stochastic controlled averaging for federated learning. In *International Conference on Machine Learning*, pages 5132–5143. PMLR, 2020.
- [76] Daniel S Kermany, Michael Goldbaum, Wenjia Cai, Carolina CS Valentim, Huiying Liang, Sally L Baxter, Alex McKeown, Ge Yang, Xiaokang Wu, Fangbing Yan, et al. Identifying medical diagnoses and treatable diseases by image-based deep learning. *Cell*, 172(5):1122–1131, 2018.
- [77] Diederik P Kingma and Jimmy Ba. Adam: A method for stochastic optimization. *arXiv preprint arXiv:1412.6980*, 2014.
- [78] Alex Krizhevsky, Geoffrey Hinton, et al. Learning multiple layers of features from tiny images, 2009.
- [79] Amal Lahiani, Irina Klamann, Nassir Navab, Shadi Albarqouni, and Eldad Klaiman. Seamless virtual whole slide image synthesis and validation using perceptual embedding consistency. *IEEE Journal of Biomedical and Health Informatics*, 25(2):403–411, 2020.
- [80] Fan Lai, Yinwei Dai, Sanjay Singapuram, Jiachen Liu, Xiangfeng Zhu, Harsha Madhyastha, and Mosharaf Chowdhury. FedScale: Benchmarking model and system performance of federated learning at scale. In *International Conference on Machine Learning*, pages 11814–11827. PMLR, 2022.
- [81] Yann LeCun and Corinna Cortes. MNIST handwritten digit database. <http://yann.lecun.com/exdb/mnist/>, 2010.
- [82] Tian Li, Anit Kumar Sahu, Ameet Talwalkar, and Virginia Smith. Federated learning: Challenges, methods, and future directions. *IEEE Signal Processing Magazine*, 37(3):50–60, 2020.
- [83] Tian Li, Anit Kumar Sahu, Manzil Zaheer, Maziar Sanjabi, Ameet Talwalkar, and Virginia Smith. Federated optimization in heterogeneous networks. *Proceedings of Machine Learning and Systems*, 2:429–450, 2020.
- [84] Wei Li and Andrew McCallum. Pachinko allocation: DAG-structured mixture models of topic correlations. In *Proceedings of the 23rd international conference on Machine learning*, pages 577–584, 2006.
- [85] Wei Yang Bryan Lim, Nguyen Cong Luong, Dinh Thai Hoang, Yutao Jiao, Ying-Chang Liang, Qiang Yang, Dusit Niyato, and Chunyan Miao. Federated learning in mobile edge networks: A comprehensive survey. *IEEE Communications Surveys & Tutorials*, 22(3):2031–2063, 2020.
- [86] Tsung-Yi Lin, Priya Goyal, Ross B. Girshick, Kaiming He, and Piotr Dollár. Focal loss for dense object detection. *CoRR*, abs/1708.02002, 2017.
- [87] Geert Litjens, Peter Bandi, Babak Ehteshami Bejnordi, Oscar Geessink, Maschenka Balkenhol, Peter Bult, Altuna Halilovic, Meyke Hermsen, Rob van de Loo, Rob Vogels, et al. 1399 H&E-stained sentinel lymph node sections of breast cancer patients: the CAMELYON dataset. *GigaScience*, 7(6):giy065, 2018.
- [88] Ziwei Liu, Ping Luo, Xiaogang Wang, and Xiaoou Tang. Deep learning face attributes in the wild. In *Proceedings of the IEEE international conference on computer vision*, pages 3730–3738, 2015.
- [89] Ming Y Lu, Richard J Chen, Dehan Kong, Jana Lipkova, Rajendra Singh, Drew FK Williamson, Tiffany Y Chen, and Faisal Mahmood. Federated learning for computational pathology on gigapixel whole slide images. *Medical image analysis*, 76:102298, 2022.
- [90] Ming Y Lu, Drew FK Williamson, Tiffany Y Chen, Richard J Chen, Matteo Barbieri, and Faisal Mahmood. Data-efficient and weakly supervised computational pathology on whole-slide images. *Nature biomedical engineering*, 5(6):555–570, 2021.

- [91] Yunlong Lu, Xiaohong Huang, Ke Zhang, Sabita Maharjan, and Yan Zhang. Low-latency federated learning and blockchain for edge association in digital twin empowered 6g networks. *IEEE Transactions on Industrial Informatics*, 17(7):5098–5107, 2020.
- [92] Jiahuan Luo, Xueyang Wu, Yun Luo, Anbu Huang, Yunfeng Huang, Yang Liu, and Qiang Yang. Real-world image datasets for federated learning. *arXiv preprint arXiv:1910.11089*, 2019.
- [93] Zhengquan Luo, Yunlong Wang, Zilei Wang, Zhenan Sun, and Tieniu Tan. Fediris: Towards more accurate and privacy-preserving iris recognition via federated template communication. *CVPRW*, 2022.
- [94] Agnes Lydia and Sagayaraj Francis. Adagrad—an optimizer for stochastic gradient descent. *Int. J. Inf. Comput. Sci.*, 6(5):566–568, 2019.
- [95] Othmane Marfoq, Chuan Xu, Giovanni Neglia, and Richard Vidal. Throughput-Optimal Topology Design for Cross-Silo Federated Learning. In *34th Conference on Neural Information Processing Systems (NeurIPS 2020)*, Vancouver, Canada, December 2020. NeurIPS 2020.
- [96] Leland McInnes, John Healy, and James Melville. Umap: Uniform manifold approximation and projection for dimension reduction. *arXiv preprint arXiv:1802.03426*, 2018.
- [97] Brendan McMahan, Eider Moore, Daniel Ramage, Seth Hampson, and Blaise Aguera y Arcas. Communication-efficient learning of deep networks from decentralized data. In *Artificial intelligence and statistics*, pages 1273–1282. PMLR, 2017.
- [98] Fausto Milletari, Nassir Navab, and Seyed-Ahmad Ahmadi. V-net: Fully convolutional neural networks for volumetric medical image segmentation. In *2016 fourth international conference on 3D vision (3DV)*, pages 565–571. IEEE, 2016.
- [99] TCGA Research Network. Tensorflow federated stack overflow dataset. <https://www.cancer.gov/tcga>. Accessed: 2022-05-18.
- [100] Adaloglou Nikolaos. Deep learning in medical image analysis: a comparative analysis of multi-modal brain-mri segmentation with 3d deep neural networks. Master’s thesis, University of Patras, 2019. <https://github.com/black0017/MedicalZooPytorch>.
- [101] Chaoyue Niu, Fan Wu, Shaojie Tang, Lifeng Hua, Rongfei Jia, Chengfei Lv, Zhihua Wu, and Guihai Chen. Billion-scale federated learning on mobile clients: a submodel design with tunable privacy. In *Proceedings of the 26th Annual International Conference on Mobile Computing and Networking*, pages 1–14, 2020.
- [102] Adam Paszke, Sam Gross, Francisco Massa, Adam Lerer, James Bradbury, Gregory Chanan, Trevor Killeen, Zeming Lin, Natalia Gimelshein, Luca Antiga, et al. Pytorch: An imperative style, high-performance deep learning library. *Advances in neural information processing systems*, 32, 2019.
- [103] Sarthak Pati, Ujjwal Baid, Maximilian Zenk, Brandon Edwards, Micah Sheller, G Anthony Reina, Patrick Foley, Alexey Gruzdev, Jason Martin, Shadi Albarqouni, et al. The federated tumor segmentation (FeTS) challenge. *arXiv preprint arXiv:2105.05874*, 2021.
- [104] Fernando Pérez-García, Rachel Sparks, and Sebastien Ourselin. Torchio: a python library for efficient loading, preprocessing, augmentation and patch-based sampling of medical images in deep learning. *Computer Methods and Programs in Biomedicine*, 208:106236, 2021.
- [105] Constantin Philippenko and Aymeric Dieuleveut. Bidirectional compression in heterogeneous settings for distributed or federated learning with partial participation: tight convergence guarantees. *arXiv preprint arXiv:2006.14591*, 2020.
- [106] P Jonathon Phillips, Kevin W Bowyer, Patrick J Flynn, Xiaomei Liu, and W Todd Scruggs. The iris challenge evaluation 2005. In *2008 IEEE Second International Conference on Biometrics: Theory, Applications and Systems*, pages 1–8. IEEE, 2008.
- [107] unet 0.7.7. <https://pypi.org/project/unet/0.7.7/>. Accessed: 2022-02-02.

- [108] Fernando Pérez-García. Ixitiny dataset. <https://torchio.readthedocs.io/datasets.html#torchio.datasets.ixi.IXITiny>. Accessed: 2022-05-18.
- [109] Aditya Ramesh, Prafulla Dhariwal, Alex Nichol, Casey Chu, and Mark Chen. Hierarchical text-conditional image generation with clip latents, 2022.
- [110] Sashank Reddi, Zachary Charles, Manzil Zaheer, Zachary Garrett, Keith Rush, Jakub Konečný, Sanjiv Kumar, and H Brendan McMahan. Adaptive federated optimization. *arXiv preprint arXiv:2003.00295*, 2020.
- [111] Meta AI Research. Federated learning simulator (flsim). <https://github.com/facebookresearch/FLSim/tree/main/examples>, 2012.
- [112] Nicola Rieke, Jonny Hancox, Wenqi Li, Fausto Milletari, Holger R Roth, Shadi Albarqouni, Spyridon Bakas, Mathieu N Galtier, Bennett A Landman, Klaus Maier-Hein, et al. The future of digital health with federated learning. *NPJ digital medicine*, 3(1):1–7, 2020.
- [113] Felix Sattler, Simon Wiedemann, Klaus-Robert Müller, and Wojciech Samek. Sparse binary compression: Towards distributed deep learning with minimal communication. In *2019 International Joint Conference on Neural Networks (IJCNN)*, pages 1–8. IEEE, 2019.
- [114] Arnaud Arindra Adiyoso Setio, Alberto Traverso, Thomas De Bel, Moira SN Berens, Cas Van Den Bogaard, Piergiorgio Cerello, Hao Chen, Qi Dou, Maria Evelina Fantacci, Bram Geurts, et al. Validation, comparison, and combination of algorithms for automatic detection of pulmonary nodules in computed tomography images: the LUNA16 challenge. *Medical image analysis*, 42:1–13, 2017.
- [115] Micah J Sheller, Brandon Edwards, G Anthony Reina, Jason Martin, Sarthak Pati, Aikaterini Kotrotsou, Mikhail Milchenko, Weilin Xu, Daniel Marcus, Rivka R Colen, et al. Federated learning in medicine: facilitating multi-institutional collaborations without sharing patient data. *Scientific reports*, 10(1):1–12, 2020.
- [116] Micah J Sheller, G Anthony Reina, Brandon Edwards, Jason Martin, and Spyridon Bakas. Multi-institutional deep learning modeling without sharing patient data: A feasibility study on brain tumor segmentation. In *International MICCAI Brainlesion Workshop*, pages 92–104. Springer, 2018.
- [117] Santiago Silva, Andre Altmann, Boris Gutman, and Marco Lorenzi. Fed-BioMed: A general open-source frontend framework for federated learning in healthcare. In *Domain Adaptation and Representation Transfer, and Distributed and Collaborative Learning*, pages 201–210. Springer, 2020.
- [118] Chen Sun, Abhinav Shrivastava, Saurabh Singh, and Abhinav Gupta. Revisiting unreasonable effectiveness of data in deep learning era. In *Proceedings of the IEEE international conference on computer vision*, pages 843–852, 2017.
- [119] Mingxing Tan and Quoc V. Le. Efficientnet: Rethinking model scaling for convolutional neural networks. *CoRR*, abs/1905.11946, 2019.
- [120] Tensorflow. Tensorflow federated stack overflow dataset. https://www.tensorflow.org/federated/api_docs/python/tff/simulation/datasets/stackoverflow/load_data, 2019.
- [121] Katarzyna Tomczak, Patrycja Czerwińska, and Maciej Wiznerowicz. The cancer genome atlas (TCGA): an immeasurable source of knowledge. *Contemporary oncology*, 19(1A):A68, 2015.
- [122] Antonio Torralba and Alexei A Efros. Unbiased look at dataset bias. In *CVPR 2011*, pages 1521–1528. IEEE, 2011.
- [123] Philipp Tschandl, Cliff Rosendahl, and Harald Kittler. The HAM10000 dataset, a large collection of multi-source dermatoscopic images of common pigmented skin lesions. *Scientific data*, 5(1):1–9, 2018.

- [124] Laurens Van der Maaten and Geoffrey Hinton. Visualizing data using t-SNE. *Journal of machine learning research*, 9(11), 2008.
- [125] G. Van Horn, O. Mac Aodha, Y. Song, Y. Cui, C. Sun, A. Shepard, H. Adam, P. Perona, and S. Belongie. The inaturalist species classification and detection dataset. In *2018 IEEE/CVF Conference on Computer Vision and Pattern Recognition*, pages 8769–8778, 2018.
- [126] Mitko Veta, Josien PW Pluim, Paul J Van Diest, and Max A Viergever. Breast cancer histopathology image analysis: A review. *IEEE transactions on biomedical engineering*, 61(5):1400–1411, 2014.
- [127] Michael Völske, Martin Potthast, Shahbaz Syed, and Benno Stein. TL;DR: Mining Reddit to learn automatic summarization. In *Proceedings of the Workshop on New Frontiers in Summarization*, pages 59–63, Copenhagen, Denmark, September 2017. Association for Computational Linguistics.
- [128] Zhuoshi Wei, Tieniu Tan, and Zhenan Sun. Nonlinear iris deformation correction based on gaussian model. In *International Conference on Biometrics*, pages 780–789. Springer, 2007.
- [129] Qi Xia, Winson Ye, Zeyi Tao, Jindi Wu, and Qun Li. A survey of federated learning for edge computing: Research problems and solutions. *High-Confidence Computing*, page 100008, 2021.
- [130] Guoyang Xie, Jinbao Wang, Yawen Huang, Yefeng Zheng, Feng Zheng, Jingkuang Song, and Yaochu Jin. FedMed-GAN: Federated multi-modal unsupervised brain image synthesis. *arXiv preprint arXiv:2201.08953*, 2022.
- [131] Haibo Yang, Minghong Fang, and Jia Liu. Achieving linear speedup with partial worker participation in non-iid federated learning. *arXiv preprint arXiv:2101.11203*, 2021.
- [132] Bill Yuchen Lin, Chaoyang He, Zihang Zeng, Hulin Wang, Yufen Huang, Christophe Dupuy, Rahul Gupta, Mahdi Soltanolkotabi, Xiang Ren, and Salman Avestimehr. Fednlp: Benchmarking federated learning methods for natural language processing tasks. *Findings of NAACL*, 2022.
- [133] Mikhail Yurochkin, Mayank Agarwal, Soumya Ghosh, Kristjan Greenewald, Nghia Hoang, and Yasaman Khazaeni. Bayesian nonparametric federated learning of neural networks. In *International Conference on Machine Learning*, pages 7252–7261. PMLR, 2019.
- [134] Manzil Zaheer, Sashank Reddi, Devendra Sachan, Satyen Kale, and Sanjiv Kumar. Adaptive methods for nonconvex optimization. *Advances in neural information processing systems*, 31, 2018.
- [135] Hui Zhang, Zhenan Sun, and Tieniu Tan. Contact lens detection based on weighted lbp. In *2010 20th International Conference on Pattern Recognition*, pages 4279–4282. IEEE, 2010.
- [136] Qi Zhang, Haiqing Li, Zhenan Sun, and Tieniu Tan. Deep feature fusion for iris and periocular biometrics on mobile devices. *IEEE Transactions on Information Forensics and Security*, 13(11):2897–2912, 2018.

Checklist

1. For all authors...
 - (a) Do the main claims made in the abstract and introduction accurately reflect the paper’s contributions and scope? [\[Yes\]](#)
 - (b) Did you describe the limitations of your work? [\[Yes\]](#) See Section 5.
 - (c) Did you discuss any potential negative societal impacts of your work? [\[Yes\]](#) See Section A.
 - (d) Have you read the ethics review guidelines and ensured that your paper conforms to them? [\[Yes\]](#) We point out that we not collect data ourselves. We did a thorough background check on each dataset regarding compliance with these guidelines. We refer to the detailed appendix of each dataset for specific details.
2. If you are including theoretical results...
 - (a) Did you state the full set of assumptions of all theoretical results? [\[N/A\]](#) Our work does not contain theoretical results.
 - (b) Did you include complete proofs of all theoretical results? [\[N/A\]](#) Our work does not contain theoretical results.
3. If you ran experiments (e.g. for benchmarks)...
 - (a) Did you include the code, data, and instructions needed to reproduce the main experimental results (either in the supplemental material or as a URL)? [\[Yes\]](#) See Abstract.
 - (b) Did you specify all the training details (e.g., data splits, hyperparameters, how they were chosen)? [\[Yes\]](#) See supplementary and code provided.
 - (c) Did you report error bars (e.g., with respect to the random seed after running experiments multiple times)? [\[Yes\]](#) We reported error bars as we report the average error on the local test sets across multiple seeds. For the largest one, we did not use multiple seeds, but observed empirically a smaller variance in the results due to larger local test set sizes.
 - (d) Did you include the total amount of compute and the type of resources used (e.g., type of GPUs, internal cluster, or cloud provider)? [\[Yes\]](#) See Appendix J.1
4. If you are using existing assets (e.g., code, data, models) or curating/releasing new assets...
 - (a) If your work uses existing assets, did you cite the creators? [\[Yes\]](#) See Section 3.
 - (b) Did you mention the license of the assets? [\[Yes\]](#) See code and supplementary.
 - (c) Did you include any new assets either in the supplemental material or as a URL? [\[Yes\]](#) See link in abstract.
 - (d) Did you discuss whether and how consent was obtained from people whose data you’re using/curating? [\[Yes\]](#) We are only repurposing existing assets. We did a thorough background check on each dataset on this issue. We refer to the detailed appendix of each dataset for specific details.
 - (e) Did you discuss whether the data you are using/curating contains personally identifiable information or offensive content? [\[Yes\]](#) We are only repurposing existing assets. We did a thorough background check on each dataset on this issue. We refer to the detailed appendix of each dataset for specific details.
5. If you used crowdsourcing or conducted research with human subjects...
 - (a) Did you include the full text of instructions given to participants and screenshots, if applicable? [\[N/A\]](#) We are only repurposing existing assets.
 - (b) Did you describe any potential participant risks, with links to Institutional Review Board (IRB) approvals, if applicable? [\[N/A\]](#) We are only repurposing existing assets.
 - (c) Did you include the estimated hourly wage paid to participants and the total amount spent on participant compensation? [\[N/A\]](#) We are only repurposing existing assets.

A Broader Impact

As this study solely involves the repurposing of existing open-source materials and benchmarking, there are limited risks associated within the study itself. However, it should be noted that all datasets included in this study could be subject to biases originated during the collection process, such as gender or ethnicity biases. Unfortunately, on the images' datasets (5 datasets out of 7), the sources of such potential biases cannot be easily checked, since data were properly pseudonymised and image-based medical records cannot be straightforwardly tied back to a particular ethnicity or gender by non-medical experts. Nevertheless, as our work exposes more clearly some metadata (e.g. geographical origin) of the datasets, it might help revealing underlying geographical biases, and thus help building more heterogeneous benchmarks, as expected in real scenarios for FL.

As we focused on simplicity and ease of use, the current benchmark does not encompass privacy metrics. However, privacy is of paramount importance in healthcare cross-silo FL, and we urge the community not to ignore these aspects. Thanks to the modularity of FLamby, it is easy to add privacy components, as we show in a DP example in Appendix L.1. Thus, we hope FLamby will help tackle privacy questions in healthcare cross-silo FL.

B Datasets repository and Authors Statement

B.1 Dataset repository.

The code is now available at <https://github.com/owkin/FLamby>

The code respects best practices for reproducibility and dataset sharing. The installation process is detailed and allows to install only requirements of specific datasets. Regarding code readability, the code is linted with black and flake8 and most functions have docstrings. Documentation is automatically generated from markdown with sphinx, including tutorials. Unit tests ensure FL strategies perform correctly.

Regarding licenses, all datasets documented in this repository come with links towards data terms or licenses. Every time a user downloads a dataset for the first time, he or she is prompted with a link towards the data terms or license, and has to explicitly agree to it in order to proceed.

B.2 Maintenance plan

We will follow a maintenance plan to ensure the code remains correct and the datasets provided by the suite follow adequate standards. In particular, this maintenance plan encompasses:

- Fixing bugs affecting the correctness of the code, whether brought out by the community or ourselves;
- Ensuring security updates in the dependencies are performed;
- Regarding datasets, reviewing, on a monthly basis, potential updates of the datasets referenced in the suite, including but not limited to patients opting out or ethical concerns raised by the work. Such modification may go to the extent of a full revocation of the related dataset if need be;
- Reviewing contributions from the community, whether they are related to the benchmark or to incorporating new datasets to the suite, ensuring they are at the highest standards.

B.3 Authors statement.

As authors of this repository and article we bear all responsibility in case of violation of rights and licenses. We have added a disclaimer on the repository to invite original datasets creators to open issues regarding any license related matters.

Table 2: Information for the different clients in Camelyon16

Number	Client	Dataset size	Train	Test
0	RUMC	243	169	74
1	UMCU	156	101	55

C Fed-Camelyon16

C.1 Description

Camelyon16 [LBEB⁺18] is a histopathology dataset of 399 digitized breast biopsies’ slides with or without tumor collected from two hospitals: Radboud University Medical Center (RUMC) and University Medical Center Utrecht (UMCU). The client information can be read directly from the training slides as the first 170 slides belong to RUMC and the others to UMCU. For the test slides we use a manual approach based on clustering to recover the centres and visual inspection. The slides split are summarized Table 2

C.2 License and Ethics

The Camelyon data is open access (CC0)¹.

The collection of the data was approved by the local ethics committee (Commissie Mensgebonden Onderzoek regio Arnhem - Nijmegen) under 2016-2761, and the need for informed consent was waived [LBEB⁺18].

C.3 Download and preprocessing

As the original dataset is stored in Google Drive, we provide code relying on the Google drive API’s python SDK to batch download all the images (800GB) efficiently. It requires the user to have a Google account and to setup a service account. Detailed instructions are provided in the repository.

Once all tif images have been downloaded we use the histolab package[MAB] to tile the slides with patches of size 224x224 at the second level of the image pyramid corresponding to $\approx 0.5 \mu\text{m} / \text{pixel}$. We only keep tiles with sufficient amount of tissue on them thanks to the `check_tissue=True` option of the `GridTiler` histolab object. We then perform Imagenet preprocessing [HZRS16] and extract a 2048 feature vector from an Imagenet-pretrained Resnet50 [HZRS16] on each patch. As slides have different amount of matter this produces a variable number of features per slide. We subsequently save those features in the numpy format [VDWCV11].

C.4 Task

Each of this slide represented as a bag of features has a binary label indicating the presence of a tumour on the breast. The task is to predict if a slide contains a tumour or not so it is framed as a binary classification problem under the Multiple Instance Learning paradigm[ITW].

C.5 Baseline, loss function and evaluation

Loss function We use a traditional binary cross entropy loss [Goo92] and evaluate the performance with the Area under the ROC curve or AUC [Bra97].

Baseline Model We use the DeepMIL[ITW] architecture that uses attention to learn to weight patch features importance in an end to end fashion. The network architecture is specified in the code. The model trains in approximately 5 minutes on a P100.

¹<https://camelyon17.grand-challenge.org/Data/>

Optimization parameters We use a batch size of 16 with Adam [KB14] with a learning rate of 0.001. Both sets of hyperparameters mentioned above used for the network architecture and optimization are taken from [DCM⁺20], we change the number of pooled epochs to 45 in order to be able to do more than one synchronization rounds when performing federated experiments.

Hyperparameter Search For the pooled dataset benchmark we use the configuration described above without further tuning. For FL strategies we use the following hyperparameter grid: for clients’ learning rates (all strategies) {1e-5, 1e-4, 1e-3, 1e-2, 1e-1, 1.0}; for server size learning rate (for Scaffold and FedOpt strategies) {1e-3, 1e-2, 1e-1, 1.0, 10.0}, and for FedProx only, μ belongs to {1e-2, 1e-1, 1.0}.

D Fed-LIDC-IDRI

D.1 Description

LIDC-IDRI [AIMB⁺11, IMB⁺15, CVS⁺13] is part of The Cancer Imaging Archive (TCIA) database [CVS⁺13] with 1009 lung CT-scans (3D images), on which radiologists annotated the presence of nodules.

We split the dataset in 4 different clients that correspond to different medical imagery machine manufacturers, which were previously shown to be a source of heterogeneity in CT image quality [FDZ⁺15]. We end up with 661 samples gathered by GE Medical Systems, 205 by Siemens, 69 by Toshiba, and 74 by Philips scanner. These datasets are further split in training and testing sets that contain respectively 80% and 20% of the data. This split is stratified according to clients, so that proportions are respected. The exact distribution of the samples between clients are given in Table 3

Table 3: Information for the different clients in LIDC IDRI.

Number	Client	Dataset size	Train	Test
0	GE MEDICAL SYSTEMS	661	530	131
1	Philips	74	59	15
2	SIEMENS	205	164	41
3	TOSHIBA	69	55	14

D.2 License and Ethics

The users of this data must abide by the Data Usage Policies listed on the TCIA webpage under LIDC (links are provided in the README of the LIDC dataset in FLamby repository). It is licensed under a Creative Commons Attribution 3.0 Unported License.

Data was anonymized in each local center before being uploaded to the central repository [AIMB⁺11]. Further, as per the terms of use of TCIA², “users must agree not to generate and use information in a manner that could allow the identities of research participants to be readily ascertained”.

D.3 Download and preprocessing

Instructions in the README.md of the LIDC-IDRI dataset in FLamby repository allow to download images and average annotation masks from the TCIA initiative. Flamby code then permits conversion from DICOMs to nifti files to facilitate further analysis.

D.3.1 Preprocessing and sampling

Raw CT scans have varying dimensions which must be standardized prior to training. Therefore, as a first step we resize them to a common (384, 384, 384) shape by cropping dimensions in excess and

²<https://wiki.cancerimagingarchive.net/display/Public/Data+Usage+Policies+and+Restrictions>

reflection-padding missing dimensions. During training, this operation is performed in the same way both on the CT scans and the ground truth masks.

Next, the images are normalized. CT scan voxels are originally expressed in the Hounsfield unit (HU) [Fee10] scale: roughly $-1,000$ HU for air, 0 HU for water, and $1,000$ HU for bone. We clip the images to the $[-1024, 600]$ range, add 1024 , and then divide voxels by 1624 to obtain values ranging in $[0, 1]$.

D.4 Task

We benchmark federated learning strategies on a nodule segmentation task using a VNet [MNA16]. More precisely, we aim to maximize the DICE coefficient [Dic45] between predictions and the annotated ground truths. For reference, the baseline model trained on the pooled training set achieves a DICE of 41% on the pooled test set.

D.5 Baseline, loss function and evaluation

Sampling The resulting images of size $(384, 384, 384)$ are too voluminous to fit in the memory of most GPUs. Hence, during training we feed the model with sampled patches of size $(128, 128, 128)$. We sample 2 patches from each (image, mask) pair. This implies that batches are constituted of two $(128, 128, 128)$ patches drawn from the same CT scan. As lung nodules are relatively small and rare, there is a strong class imbalance in the LIDC dataset. To alleviate this issue, we ensure that one of the sampled patches contains nodule voxels (by centering it on a nodule voxel drawn at random), and sample the other completely at random. To account for possible nodules at the edges of CT scans, a padding of half the patch size is applied to each dimension of the image prior to sampling.

Loss function Our objective is to maximize the DICE coefficient [Dic45]. However, we observed that maximizing DICE alone during training yielded poor results at inference time on regions that do not contain nodules. To force the model to account for class imbalance, we added a small balanced cross-entropy term [see Jad20]. Hence, we minimize the following loss:

$$\mathcal{L}(\mathbf{y}, \hat{\mathbf{y}}) = (1 - \text{DICE}(\mathbf{y}, \hat{\mathbf{y}})) + 0.1 \times \text{BCE}(\mathbf{y}, \hat{\mathbf{y}}), \quad (2)$$

with

$$\text{DICE}(\mathbf{y}, \hat{\mathbf{y}}) = \frac{2 \sum_{i=1}^n y_i \hat{y}_i}{\sum_{i=1}^n y_i + \sum_{i=1}^n \hat{y}_i}, \quad (3)$$

and

$$\text{BCE}(\mathbf{y}, \hat{\mathbf{y}}) = -\alpha \sum_{i=1}^n y_i \log(\hat{y}_i) - \sum_{i=1}^n (1 - y_i) \log(1 - \hat{y}_i), \quad (4)$$

where $\alpha = (\max(\frac{1}{n} \sum_{i=1}^n y_i, 10^{-7}))^{-1} - 1$.

Baseline Model We implement a VNet [MNA16], following the architecture proposed therein. During training, we use dropout ($p = 0.25$). The final layer produces a single output, which is passed through a sigmoid function to encode the probability that each voxel corresponds to a nodule. The model trains in approximately 48 hours on a P100.

Optimization parameters We optimize the VNet using RMSprop, with an initial learning rate of 10^{-2} . We run 100 epochs, multiplying the learning rate by 0.95 every 10 epochs.

Hyperparameters search LIDC FL trainings take approximately 70 hours on a P100 so because of time constraints we could not use an extensive grid search as for other datasets. The final parameters we use are reported in Section J.3.

E Fed-IXI

E.1 Description

IXI Tiny [PG] is a light version of the dataset IXI, a multimodal brain imaging dataset of almost 600 subjects [dt]. This lighter version provides T1-weighted brain MR images for a subset of 566 subjects,

Table 4: Demographics information for Fed-IXI.

Hospital Name	Sex	Dataset size	Age	Age Range
Guys	Female	184	53.23 ± 15.25	20 - 80
	Male	144	51.02 ± 17.26	20 - 86
HH	Female	93	50.28 ± 16.93	20 - 81
	Male	85	44.43 ± 15.67	20 - 73
IOP	Female	44	43.90 ± 18.43	19 - 86
	Male	24	39.57 ± 12.46	23 - 70

along with a set of corresponding brain image segmentations labels, taking the form of binary image masks.

Brain image masks isolate the brain pixels from the other head components, such as the eyes, skin, and fat. For the supervised task, brain image segmentation masks (labels) were obtained through automatic whole-brain extraction on the T1-weighted MRI data, using the unsupervised brain extraction tool ROBEX [ILTT11].

The images come from three different London hospitals: Guys (Guy’s Hospital, manufacturer code 0), HH (Hammersmith Hospital, manufacturer code 1), both using a Philips 1.5T system, and IOP (Institute of Psychiatry, manufacturer code 2), using a GE 1.5T system. We split this dataset in training and testing sets, respectively containing 80% and 20% of the data. The split is also stratified according to hospitals to preserve data proportions. In other words, we define one test set on each hospital. Table 4 provides demographic information for this dataset.

E.2 License and Ethics

This dataset is licensed under a Creative Commons Attribution Share Alike 3.0 Unported (CC BY-SA 3.) license.

The dataset website does not provide any information regarding data collection ethics. However, the original dataset was collected as part of the IXI - Information eXtraction from Images (EPSRC GR/S21533/02) project, and thus funded by UK Research and Innovation (UKRI). As part of its terms and conditions³, the UKRI demands that all funded projects are “carried out in accordance with all applicable ethical, legal and regulatory requirements” (RGC 2.2).

E.3 Downloading and preprocessing

We provide a helper script to download the dataset from an Amazon S3 bucket.

Preprocessing and sampling We use a fixed preprocessing step that is performed once. Brain scans are first geometrically aligned to a common anatomical space (MNI template) through affine registration estimated with NiftyReg [Mod]. Images are then reoriented using ITK [MLI⁺14]. Finally, intensities are normalized in each image (based on the entire image histogram), and the image volumes are resized from 83x44x55 to 48x60x48 voxels.

E.4 Task

The task is to segment the brain on the volume. The prediction is evaluated with the DICE score, which is the symmetric of the DICE loss with respect to 1/2.

³<https://www.ukri.org/wp-content/uploads/2022/04/UKRI-050422-FullEconomicCostingGrantTermsConditions-Apr2022.pdf>

E.5 Baseline, loss function and evaluation

Loss function The model was directly trained for the DICE loss [Dic45], defined as

$$\ell_{DICE} = 1 - S_{DICE} = 1 - \frac{2TP}{2TP + FP + FN + \epsilon},$$

where TP, FP, and FN stand for the true positive rate, false positive rate, and false negative rate, respectively, and $\epsilon = 10^{-9}$ ensures numerical stability.

Baseline Model We use a UNet model taking the individual T1 image as input, to predict the associated binary brain mask. The UNet model is a standard type of convolution neural network architecture commonly used in biomedical image segmentation tasks [RFB15]. It is specifically used to perform semantic segmentation, meaning that each voxel of the image volume is classified. We can also refer to this task as a dense prediction. The model trains in approximately 5 minutes on a P100.

Optimization parameters The UNet is optimized with a batch size of 2 and a learning rate of 10^{-3} with the AdamW optimizer. The best architecture used batch normalization, max-pooling, linear upsampling, zero-padding of size 1, PReLU activation functions, and 3 encoding blocks.

Hyperparameters search We do not change parameters for the pooled baseline. For FedAvg and Cyclic, we optimized the learning rate over the values $\{0.1, 0.01, 0.001, 0.0001, 0.00001\}$. For FedYogi, FedAdam, FedAdagrad and Scaffold, our search grid space was $\{0.1, 0.01, 0.001, 0.0001, 0.00001\}$ and $\{10, 1, 0.1, 0.01, 0.001\}$ for the learning rate and the server learning rate respectively. For FedProx, our search space contained $\{0.1, 0.01\}$ and $\{1, 0.1, 0.01\}$ sets for learning rate and μ respectively.

F Fed-TCGA-BRCA

F.1 Description

Our dataset comes from The Cancer Genome Atlas (TCGA)’s Genomics Data Commons (GDC) portal [Net] more specifically from the BREast CAncer study (BRCA), which includes features gathered from 1066 patients. We use the material produced by Liu *et al.* [LLH⁺18] as a base file that we further preprocess with one-hot encoding following [AMM⁺20]. This produces a lightweight tabular dataset with 39 input features. Patients’ labels are overall survival time and event status with the event being death. We use the Tissue Source Site metadata to split data based on extraction site, grouped into geographic regions to obtain large enough clients. We end up with 6 clients: USA (Northeast, South, Middlewest, West), Canada and Europe, with patient counts varying from 51 to 311. Our train-test split of the data is stratified per client and event. Table 5 provides details per client for this dataset. Table 6 provides results of pair-wise log-rank tests between the different clients.

F.2 License and Ethics

The data terms can be found on the GDC website⁴. In particular, these terms bind users as to “not attempt to identify individual human research participants from whom the data were obtained”.

As per the TCGA policies⁵, special care was devoted to ensure privacy protection of research subjects, including but not limited to HIPAA compliance. Note that we do not use the genetic part of TCGA whose access is restricted due to its sensitivity.

F.3 Downloading and preprocessing

The pooled TCGA-BRCA dataset requires no downloading or extra-preprocessing as the preprocessed data is now a part of the Flamby repository.

⁴<https://gdc.cancer.gov/access-data/data-access-processes-and-tools>

⁵<https://www.cancer.gov/about-nci/organization/ccg/research/structural-genomics/tcga/history/policies>

Table 5: Information for the different clients (geographical regions) in Fed-TCGA-BRCA.

Number	Client	Dataset size	Train	Test	Censorship ratio
0	USA Northeast	311	248	63	81
1	USA South	196	156	40	80
2	USA West	206	164	42	89
3	USA Midwest	162	129	33	88
4	Europe	162	129	33	94
5	Canada	51	40	11	94

Table 6: Pairwise log-rank p -values on the Fed-TCGA-BRCA clients. Some clients have significant differences for a 10% significance threshold.

Compared with	Client 1	Client 2	Client 3	Client 4	Client 5
Client 0	0.289682	0.066374	0.039892	0.576926	0.200366
Client 1		0.192075	0.161797	0.92917	0.541251
Client 2			0.954475	0.720912	0.256973
Client 3				0.576374	0.127662
Client 4					0.441106

F.4 Task

The task consists in predicting survival outcomes [Jen05] based on the patients’ clinical tabular data (39 features overall). This survival task is akin to a ranking problem with the score of each sample being known either directly or only by lower bound. Indeed, some patients leave the study before the event of interest is observed, and are labelled as right-censored. Survival analysis aims at solving this type of ranking problem while leveraging right-censored data. The censoring ratio in the TCGA-BRCA study is 86%.

The ranking is evaluated by using the concordance index (C-index) that measures the percentage of correctly ranked pairs while taking censorship into account:

$$C - \text{index} = \mathbb{E}_{\substack{i:\delta_i=1 \\ j:t_j>t_i}} [\mathbb{1}_{\{\eta_j < \eta_i\}}] \quad (5)$$

where η_i is a risk score assigned by our model to a patient i . In our case of linear Cox proportional hazard models we use $\eta_i = \beta^T x_i$, where x_i are the features for patient i and β the learned weights, see Section F.5.

Optimization parameters For the pooled dataset benchmark, we use the Adam optimizer [KB14], with a learning rate of 0.1 and a batch size of 8 for 30 epochs.

F.5 Baseline, loss function and evaluation

Survival analysis background Let T be the random time-to-death taken from the patient’s population under study. The survival function S is defined as:

$$S(t) = Pr[T > t] \quad (6)$$

A patient is characterized by its vector of covariates x (clinical data in our case), an observed time point t and an indicator $\delta \in \{0, 1\}$ where $\delta = 0$ if the event has been censored. A key quantity characterizing the distribution of S is the hazard function h . It is the instantaneous rate of occurrence of the event given that it has not yet happened for a patient:

$$h(t, x) = \lim_{dt \rightarrow 0} \frac{Pr[t < T < t + dt | x, T > t]}{dt} \quad (7)$$

Loss function The simplest model in survival analysis is the linear Cox proportional hazard [Cox72]. This model assumes:

$$h(t, x) = h_0(t) \exp(\beta^T x) \quad (8)$$

where h_0 is the baseline hazard function (common to all patients and dependent on time only) and β is the vector of parameters of our linear model. β is estimated by minimization of the negative Cox partial log-likelihood, which compares relative risk ratios:

$$L(\beta) = - \sum_{i:\delta_i=1} \left[\beta^T x_i - \log \left(\sum_{j:t_j \geq t_i} \exp(\beta^T x_j) \right) \right] \quad (9)$$

where i and j index patients.

We minimize the negative Cox partial log-likelihood by gradient descent w.r.t. β .

As explained in [AMM⁺20] the Cox partial log-likelihood is not separable with respect to the samples: this means it cannot be expressed as a sum of terms each dependent on a single sample. Hence it is not separable with respect to the clients either. In this work, for simplicity, we decide to ignore this fact in the baseline: we treat each client’s negative Cox partial log-likelihood independently of the others and apply any federated learning strategy logic to the resulting local gradients. Please refer to [AMM⁺20] for a more rigorous treatment of the federated survival analysis problem.

Baseline Model As a baseline, we use the aforementioned linear Cox proportional hazard model [Cox72]. The model trains in a matter of seconds on modern CPUs.

Hyperparameter Search All the federated learning strategies are tested with the SGD optimizer. We performed a grid search for the federated learning strategies hyperparameters. For FedAvg and Cyclic, we optimized the learning rate over the values {0.1, 0.01, 0.001, 0.0001, 0.00001}. For FedYogi, FedAdam, FedAdagrad and Scaffold, our search grid space was {0.1, 0.01, 0.001, 0.0001, 0.00001} and {10, 1, 0.1, 0.01, 0.001} for the learning rate and the server learning rate respectively. For FedProx, our search space contained {0.1, 0.01} and {1, 0.1, 0.01} sets for learning rate and μ respectively. The chosen hyperparameters from the HP search can be found in Section J.3.

G Fed-KiTS19

G.1 Description

The KiTS19 dataset [HIMH⁺20, HSK⁺19] stems from the Kidney Tumor Segmentation Challenge 2019 and contains CT scans of 210 patients along with the segmentation masks from 77 hospitals⁶. We only consider the training dataset of this challenge as the segmentation masks are not provided for the test dataset. We recover the hospital metadata and extract a 6-client federated version of this dataset by removing hospitals with less than 10 training samples. Figures 3a and 3b show the repartition of patients per client before and after this client selection respectively. Table 7 provides further details of the train and test split at each selected client.

G.2 License and Ethics

This dataset is licensed under a Attribution-NonCommercial-ShareAlike 4.0 International (CC-BY-NC-SA) license⁷.

The dataset collection was approved by the Institutional Review Board at the University of Minnesota as Study 1611M00821 [HSK⁺19].

⁶It is important to note that KiTS19 dataset does not come with the hospital information. We obtained the data distribution per client from one of the organizers of this challenge, Nicholas Heller, over email communication. We acknowledge the help of Nicholas Heller for sharing this valuable resource with us that helped us explore federated learning strategies with this dataset for the first time.

⁷<https://github.com/neheller/kits19/blob/master/LICENSE>

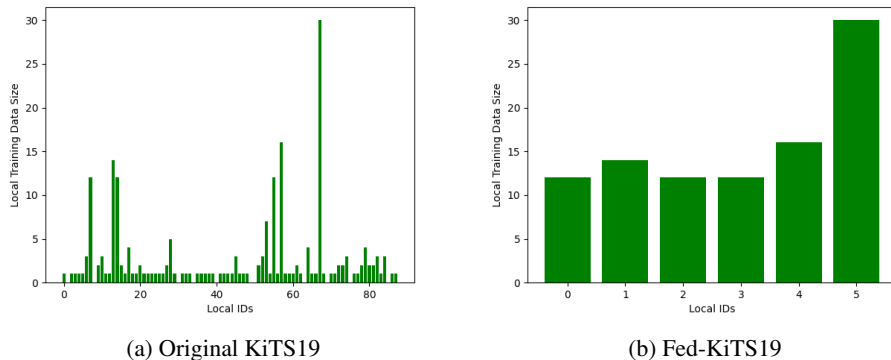


Figure 3: Patient distributions across hospitals of the original KiTS19 Dataset and the derived Data distribution of Fed-KiTS19

G.3 Downloading and Preprocessing

We use the official KiTS19 repository⁸ to download the KiTS19 data. Next, we preprocess this dataset. The first step of the preprocessing is to clip the intensity. We clip the values of each image to the [5th percentile, 95th percentile] range, where 5th percentile and 95th percentile are calculated on the image intensities of each patient’s case separately. After this step, we apply z-scale normalization, where we subtract the mean and divide by the standard deviation of the image intensities. Since KiTS19 dataset comes with inhomogeneous voxel spacing even for the patients data from the same silos, we resample the voxel spacings to the target spacing of 2.90x1.45x1.45 mm for all the samples.

G.4 Task

The task consists of both kidney and tumor segmentation, labeled 1 and 2, respectively. The background is labeled as 0. The score we consider on this dataset is the average of Kidney and Tumor DICE scores [Dic45].

G.5 Baseline, loss function and evaluation

Sampling The image size distribution of the samples of the KiTS19 dataset is heterogeneous. After the resampling detailed in section G.3, the median patient’s data size is [116, 282, 282]. To make our model’s computation memory efficient, we extract a patch of size [64, 192, 192] from each sample during the model training. The number of voxels belonging to the foreground classes (i.e. either Kidney or Tumor) is small compare to the number of voxels belonging to the background class. Therefore, we oversample the foreground classes when taking patches of the samples. More precisely, we use batches of size 2. Each batch contains one patch with the foreground oversampled. Furthermore, we split each silo’s data into training and validation data with 80% and 20% split, respectively. All this pre-processing and patching is done using the nnU-Net library [IJK⁺21].

Loss function We use the same loss function as proposed by nnU-Net [IJK⁺21] for the KiTS19 dataset which is based on DICE [Dic45] and on the Cross Entropy loss. Both losses are summed with equal weight as shown in Equation (10),

$$\mathcal{L}(\mathbf{y}, \hat{\mathbf{y}}) = \text{CE}(\mathbf{y}, \hat{\mathbf{y}}) - \text{DICE}(\mathbf{y}, \hat{\mathbf{y}}), \quad (10)$$

with

$$\text{DICE}(\mathbf{y}, \hat{\mathbf{y}}) = \frac{2 \sum_{l=1}^2 \sum_{i=1}^n y_i^l \hat{y}_i^l + \epsilon}{\sum_{l=1}^2 (\sum_{i=1}^n y_i^l + \sum_{i=1}^n \hat{y}_i^l) + \epsilon}, \quad (11)$$

⁸<https://github.com/neheller/kits19>

Table 7: Information for the selected clients in Fed-KiTS19.

Local ID Number	Dataset size	Train	Test
0	12	9	3
1	14	11	3
2	12	9	3
3	12	9	3
4	16	12	4
5	30	24	6

and

$$CE(\mathbf{y}, \hat{\mathbf{y}}) = - \sum_{i=1}^n \sum_{l=1}^2 y_i^l \log \hat{y}_i^l, \quad (12)$$

where ϵ value is $1e^{-5}$ and n is the set of all pixels and 2 signifies the 2 class labels here, Kidney and Tumor, and where y_i^l is the one-hot encoding (0 or 1) for the label l and pixel i and \hat{y}_i^l is the predicted probability for the same label l and pixel i .

Baseline Model During the training, we use nnU-Net [IJK⁺21], with the architecture proposed therein for the KiTS19 dataset. We chose convolution kernels of sizes $[[3,3,3],[3,3,3],[3,3,3],[3,3,3],[3,3,3]]$ and pool kernels of sizes $[[2,2,2],[2,2,2],[2,2,2],[2,2,2],[1,2,2]]$. The model trains in under 24 hours on a P100.

Optimization parameters In addition, we use Adam optimizer [KB14] with a learning rate of 0.0003 for 500 epochs to train our model. To evaluate the performance of the trained model, we evaluate the DICE score on the validation data for both classes, Kidney and tumor, and report the average of these two scores. We note that with 8000 epochs we can obtain higher performances, however at the expense of computational cost.

Hyperparameter Search For the pooled strategy results, we use the Adam Optimizer and 0.0003 learning rate, as used in nnU-Net work for KiTS19 dataset [IJK⁺21]. For Cyclic and FedAvg, we optimized the learning rate over the values $\{0.3, 0.03, 0.003, 0.0003, 0.00003\}$ and found that a learning rate of 0.3 provided the best results for both strategies. For FedYogi, FedAdam, FedAdagrad and Scaffold, our search grid space was $\{0.1, 0.01\}$ and $\{0.001, 0.01, 0.1, 1\}$ for the learning rate and the server learning rate respectively. In the best setting, the learning rate was 0.1 for all these strategies, and the server learning rate 0.1 for FedAdagrad, 0.01 for FedYogi and FedAdam and 1 for Scaffold. Likewise, for FedProx, our search space contained $\{0.1, 0.01\}$ and $\{0.001, 0.01, 0.1, 1\}$ sets for learning rate and μ respectively, and the best set of hyperparameters was 0.1 for the learning rate and 0.001 for μ .

H Fed-ISIC2019

H.1 Dataset description

The ISIC2019 challenge dataset [TRK18, CGC⁺18, CCR⁺19] contains 25,331 dermoscopy images collected in 4 hospitals. To the best of our knowledge, it is the largest public dataset of high-quality images of skin lesions. We restrict ourselves to 23,247 images from the public train set due to metadata availability reasons, which we re-split into train and test sets. The train-test split is static.

We split this dataset into 6 clients corresponding to different sites where images were taken with different imaging technologies. The ViDIR Group, Medical University of Vienna, Austria uses 3 different imaging systems representing evolving clinical practice: a Heine Dermaphot system using an immersion fluid, a DermLiteTM FOTO and a MoleMax HD machine which gives rise to 3 clients. On top of this, the skin cancer practice of Cliff Rosendahl in Queensland, Australia, the Hospital

Clínic de Barcelona, Spain and the Memorial Sloan Kettering Cancer Center, New York give rise to 3 other different clients making a total of 6 clients. The biggest client counts 12413 images while the smallest counts 439. Table 8 provides details about the size of the different clients.

Table 8: Information for the different clients in Fed-ISIC2019.

Number	Client	Dataset size	Train	Test
0	Hospital Clínic de Barcelona	12413	9930	2483
1	ViDIR Group, Medical University of Vienna (MoleMax HD)	3954	3163	791
2	ViDIR Group, Medical University of Vienna (DermLite FOTO)	3363	2691	672
3	The skin cancer practice of Cliff Rosendahl	2259	1807	452
4	Memorial Sloan Kettering Cancer Center	819	655	164
5	ViDIR Group, Medical University of Vienna (Heine Dermaphot)	439	351	88

H.2 License and Ethics

This dataset is licensed under a Attribution-NonCommercial 4.0 International (CC BY-NC 4.0) license⁹.

As per the terms of use of the ISIC archive¹⁰, one of the requirements for this dataset to have been hosted is that it is properly de-identified in accordance with applicable requirements and legislations.

H.3 Downloading and preprocessing

Instructions for downloading and preprocessing are available in the README of the Fed-ISIC2019 dataset inside the FLamby repository. As an offline preprocessing step, we follow recommendations and code from [Aro] by resizing images to the same shorter side of 224 pixels while maintaining their aspect ratio, and by normalizing images’ brightness and contrast through a color consistency algorithm. The total size of the raw inputs is 9 GB.

H.4 Task

The task consists in image classification among 8 different classes: Melanoma, Melanocytic nevus, Basal cell carcinoma, Actinic keratosis, Benign keratosis, Dermatofibroma, Vascular lesion and Squamous cell carcinoma. Ground truth is established through histopathology, follow-up examination, expert consensus or microscopy. The ISIC2019 dataset has a high label imbalance with prevalence ranging from 49% to less than 1% depending on the class. We follow the ISIC challenge metric: we measure classification performance through balanced accuracy, defined as the average of the recalls calculated for each class. For balanced datasets, it is equal to accuracy. A random classifier would get a balanced accuracy equal to $1/C$ where C is the number of classes. Using balanced accuracy prevents the model from taking advantage of an imbalanced test set.

H.5 Baseline, loss function and evaluation

The choices made are inspired by [Aro], [GNS⁺19], and an analysis of the solutions that scored well at the ISIC challenge over the years.

Loss function Our pretrained EfficientNet is fine-tuned using a weighted focal loss [LGG⁺17]. It is calculated as follows:

$$FL(p_t) = -\alpha_t(1 - p_t)^\gamma \log(p_t) \tag{13}$$

where p_t is the probability output by our model for the ground-truth class, α_t is the weight of the ground-truth class (a weight is attributed to each class before training), γ is a hyperparameter (chosen

⁹<https://challenge.isic-archive.com/data/>

¹⁰<https://challenge.isic-archive.com/terms-of-use/>

at 2 in our work). The focal loss is very useful where there is class imbalance. To provide an intuition behind this focal loss, compared to Binary Cross Entropy, it gives the model a bit more freedom to take some risk when making predictions. The weights we use for our weighted focal loss are the inverse of the class proportions calculated over the pooled dataset. We assume these weights are available to all clients.

Baseline Model As a baseline classification model, we fine-tune an EfficientNet [TL19]. EfficientNets are the results of a simple uniform scaling of MobileNets and ResNet on all dimensions (depth/width/resolution). They show great accuracy and efficiency and transfer very well to other tasks. Our EfficientNet is pretrained on ImageNet, we use it as a feature extractor (1280 features) by replacing the output layer by a linear layer to get an output of dimension 8. On top of this, we use the data augmentations listed below to regularize our model. The model trains in under an hour on a P100, because we have to recompute EfficientNet features with dynamic data augmentations.

For training:

1. Random Scaling
2. Rotation
3. Random Brightness Contrast
4. Flipping
5. Affine deformation
6. Random crop
7. Coarse Dropout
8. Normalization

At test time:

1. Center cropping
2. Normalization

Optimization parameters For the pooled dataset benchmark, we use the Adam optimizer [KB14] with a learning rate of 5×10^{-4} and a batch size of 64 for 20 epochs.

Hyperparameter Search All the federated learning strategies are tested with the SGD optimizer. We performed a grid search for the federated learning strategies hyperparameters. For FedAvg and Cyclic, we optimized the learning rate over the values {1e-3, 1e-2.5, 1e-2, 1e-1.5, 1e-1, 1e-0.5}. For FedYogi, FedAdam, FedAdagrad and Scaffold, our search grid space was {1e-3, 1e-2.5, 1e-2, 1e-1.5, 1e-1, 1e-0.5} and {1e-3, 1e-2.5, 1e-2, 1e-1.5, 1e-1, 1e-0.5, 1, 1e-0.5, 10} for the learning rate and the server learning rate respectively. For FedProx, our search space contained {1e-3, 1e-2.5, 1e-2, 1e-1.5, 1e-1, 1e-0.5} and {0.001, 0.01, 0.1, 1.} sets for learning rate and μ respectively. The chosen hyperparameters from the HP search can be found in Sec. J.3.

I Fed-Heart-Disease

I.1 Description

The Heart Disease dataset contains records from 920 patients from four hospitals in the USA, Hungary, and Switzerland. There are 13 features before preprocessing: age, sex, chest pain type, resting blood pressure, serum cholesterol, blood sugar, resting electrocardiographic results, maximum heart rate, exercise induced angina, ST depression induced by exercise, slope of the peak ST segment, number of major vessels, and thalassemia background. All features are continuous or binary, except for chest pain type (four categories) and resting electrocardiographic results (three categories). The target is the presence of a heart disease. After preprocessing, we are left with 740 records, each having 13 features. They are split in train and test in a stratified manner. Distribution of the data records among clients is described in Table 9.

Table 9: Distribution of data records among the different clients in Fed-Heart-Disease.

Number	Client	Dataset size	Train	Test
0	Cleveland’s Hospital	303	199	104
1	Hungarian Hospital	261	172	89
2	Switzerland Hospital	46	30	16
3	Long Beach Hospital	130	85	45

I.2 License and Ethics

This dataset is licensed under a Creative Commons Attribution 4.0 International (CC BY 4.0) license [JSPD88, DG17].

Regarding privacy, the dataset authors [JSPD88] indicated that sensitive entries of the dataset (including names and social security numbers) were removed from the database.

I.3 Downloading and Preprocessing

Instructions for downloading are available in the corresponding README file on FLamby’s repository. Dataset is downloaded from the UCI Machine Learning repository [DG17].

We preprocess the dataset by removing the three features (slope of the peak ST segment, number of major vessels, and thalassemia background) where too many entries are missing. We then remove records where at least one feature is missing. Finally, the two categorical (and non binary) features (chest pain type and resting electrocardiographic results) are encoded as binary features using dummy variables. We also normalize features per center.

I.4 Task

The task consists in predicting the presence of a heart disease so the task is binary classification.

I.5 Baseline, Loss Function, and Evaluation

Loss function For a data record (x_i, y_i) , we compute the predicted label $\hat{y}_i = \sigma(\beta^T x_i)$, where $\sigma(z) = 1/(1 + \exp(-z))$ is the sigmoid function, and β the parameters of the model. We then compute the loss over the complete dataset as

$$L(y, \hat{y}) = -\frac{1}{n} \sum_{i=1}^n y_i \log(\hat{y}_i) + (1 - y_i) \log(1 - \hat{y}_i) . \quad (14)$$

Baseline Model We fit a logistic regression model, as this is both a standard problem in medical research, and the strongest baseline according to [DG17]. The model trains in a matter of seconds on modern CPUs.

Evaluation To evaluate the model, we threshold the predicted values \hat{y} at 0.5, and measure the accuracy of the obtained labels as

$$Acc(\beta, X, y) = \frac{|\{i \in [n] \mid y_i = (\hat{y}_i > 0.5)\}|}{n} . \quad (15)$$

Optimization parameters For the pooled benchmark, we use the Adam optimizer [KB14] with a learning rate of 0.001, batch size of 4, for 50 epochs.

Hyperparameter Search All the federated learning strategies are tested with the SGD optimizer. We performed a grid search for the federated learning strategies hyperparameters . For FedAvg and Cyclic, we optimized the learning rate over the values {0.1, 0.01, 0.001, 0.0001, 0.00001}. For

Table 10: Hyperparameters used for the FedAvg strategy

FedAvg		
dataset	learning rate	optimizer
Fed-Camelyon16	0.3162	torch.optim.SGD
Fed-LIDC-IDRI	0.001	torch.optim.SGD
Fed-IXI	0.001	torch.optim.SGD
Fed-TCGA-BRCA	0.1	torch.optim.SGD
Fed-KITS19	0.03	torch.optim.SGD
Fed-ISIC2019	0.01	torch.optim.SGD
Fed-Heart-Disease	0.001	torch.optim.SGD

Table 11: Hyperparameters used for the FedProx strategy

FedProx			
dataset	mu	learning rate	optimizer
Fed-Camelyon16	0.316228	0.01	torch.optim.SGD
Fed-LIDC-IDRI	0.01	0.001	torch.optim.SGD
Fed-IXI	0.1	0.001	torch.optim.SGD
Fed-TCGA-BRCA	0.1	0.1	torch.optim.SGD
Fed-KITS19	0.001	0.1	torch.optim.SGD
Fed-ISIC2019	0.001	0.01	torch.optim.SGD
Fed-Heart-Disease	0.001	0.01	torch.optim.SGD

Table 12: Hyperparameters used for the FedAdagrad strategy

FedAdagrad						
dataset	learning rate	optimizer	learning rate server	β_1	β_2	τ
Fed-Camelyon16	0.01	torch.optim.SGD	0.003162			
Fed-LIDC-IDRI	0.1	torch.optim.SGD	0.1			
Fed-IXI	1e-04	torch.optim.SGD	0.1	0.9	0.999	1e-08
Fed-TCGA-BRCA	0.01	torch.optim.SGD	1.0	0.9	0.999	1e-08
Fed-KITS19	0.1	torch.optim.SGD	0.1	0.9	0.999	1e-08
Fed-ISIC2019	0.01	torch.optim.SGD	0.0316			
Fed-Heart-Disease	0.003162	torch.optim.SGD	0.003162	0.9	0.999	0.3162

FedYogi, FedAdam, FedAdagrad and Scaffold, our search grid space was $\{0.1, 0.01, 0.001, 0.0001, 0.00001\}$ and $\{10, 1, 0.1, 0.01, 0.001\}$ for the learning rate and the server learning rate respectively. For FedProx, our search space contained $\{0.001, 0.0001\}$ and $\{1, 0.1, 0.01\}$ sets for learning rate and μ respectively. The chosen hyperparameters from the HP search can be found in Section J.

J Experimental details

J.1 Computing resources

Most experiments were performed on virtual machines equipped with NVidia P100 GPUs in Google Cloud to tune local baselines as well as searching hyperparameters. Additional experiments were also performed on small workstations for the smallest datasets. Overall, no more than 4k GPU-hours were used throughout the full project.

J.2 FLamby experimental capabilities

FLamby is designed to be a lightweight and simple codebase, to enable ease of use. All clients run sequentially in the same python environment, without multithreading. Datasets are assigned to clients as different python objects. GPU acceleration is supported thanks to current PyTorch [PGM⁺19] back-

Table 13: Hyperparameters used for the FedAdam strategy

FedAdam						
dataset	learning rate	optimizer	learning rate server	β_1	β_2	τ
Fed-Camelyon16	0.001	torch.optim.SGD	3.1622			
Fed-LIDC-IDRI	0.3162	torch.optim.SGD	0.01			
Fed-IXI	1e-04	torch.optim.SGD	0.1	0.9	0.999	1e-08
Fed-TCGA-BRCA	0.01	torch.optim.SGD	0.1	0.9	0.999	1e-08
Fed-KITS19	0.1	torch.optim.SGD	0.01	0.9	0.999	1e-08
Fed-ISIC2019	0.01	torch.optim.SGD	0.0032			
Fed-Heart-Disease	0.01	torch.optim.SGD	0.01	0.9	0.999	1e-08

Table 14: Hyperparameters used for the FedYogi strategy

FedYogi						
dataset	learning rate	optimizer	learning rate server	β_1	β_2	τ
Fed-Camelyon16	0.003162	torch.optim.SGD	1.0			
Fed-LIDC-IDRI	0.1	torch.optim.SGD	0.001			
Fed-IXI	1e-04	torch.optim.SGD	0.1	0.9	0.999	1e-08
Fed-TCGA-BRCA	0.01	torch.optim.SGD	0.1	0.9	0.999	1e-08
Fed-KITS19	0.1	torch.optim.SGD	0.01	0.9	0.999	1e-08
Fed-ISIC2019	0.01	torch.optim.SGD	0.0032			
Fed-Heart-Disease	0.0031622	torch.optim.SGD	0.01	0.9	0.999	1e-08

Table 15: Hyperparameters used for the Cyclic strategy

Cyclic		
dataset	learning rate	optimizer
Fed-Camelyon16	0.01	torch.optim.SGD
Fed-LIDC-IDRI	0.0316	torch.optim.SGD
Fed-IXI	1e-05	torch.optim.SGD
Fed-TCGA-BRCA	0.01	torch.optim.SGD
Fed-KITS19	0.3	torch.optim.SGD
Fed-ISIC2019	0.0032	torch.optim.SGD
Fed-Heart-Disease	0.01	torch.optim.SGD

Table 16: Hyperparameters used for the Scaffold strategy

Scaffold			
dataset	learning rate	optimizer	learning rate server
Fed-Camelyon16	0.1	torch.optim.SGD	3.1622
Fed-LIDC-IDRI	0.0316	torch.optim.SGD	1.0
Fed-IXI	0.001	torch.optim.SGD	1.0
Fed-TCGA-BRCA	0.01	torch.optim.SGD	1.0
Fed-KITS19	0.1	torch.optim.SGD	1.0
Fed-ISIC2019	0.01	torch.optim.SGD	1.0
Fed-Heart-Disease	0.001	torch.optim.SGD	1.0

end. In order to perform more realistic experiments, e.g. to investigate communication constraints, we encourage the usage of dedicated FL libraries, which are easy to integrate with FLamby.

J.3 Benchmark hyperparameters

We used the hyperparameters detailed in Tables 10 to 16 to obtain the results of Figure 2. These hyperparameters were found after hyper-optimization on a coarse grid. For all strategies and datasets, we set $E = 100$ the number of local updates.

J.4 Run details

Results of Figure 2 were obtained following 5 independent runs with different random seeds, except for the largest one (Fed-LIDC-IDRI), where computational resources prevented training.

K Synthetic dataset splits

One of FLamby’s strengths is that it provides datasets with natural splits. However, due to its focus on healthcare applications, the number of clients is limited. Thanks to the standardized API of the datasets, it is possible to create new client splits based on the provided codebase.

We provide an example of such a synthetic sampling based on a Dirichlet distribution on the original clients. If K denotes the previous number of clients and K' the desired number of clients, for $\alpha \in (0, 1)$, we draw a probability distribution $\mathbf{p}_k \in \mathbb{R}^{K'}$ as

$$\mathbf{p}_k \sim \text{Dir}(\alpha), \text{ such that } \sum_{k'} p_{kk'} = 1. \tag{16}$$

Each sample from client k is then attributed to client k' with probability $p_{kk'}$, both for the train and test sets. The closer to 0 α gets, the sharper the distribution probability \mathbf{p}_k gets. In order to avoid having empty clients with the synthetic split, we recommend setting $\alpha \geq 1/2$, following previous works [YAG⁺19].

L Examples of extensions possible in FLamby

In this Appendix, we showcase the extensibility of FLamby by tackling different FL settings.

L.1 Differential Privacy Example

Differential privacy (DP) [DR⁺14] is an important approach to protect update exchanges between Federated Learning participants against malicious privacy attacks [WLL⁺20]. In this section, we use Fed-Heart-Disease to demonstrate the use of FLamby to study (ϵ, δ) -DP federated learning [DR⁺14].

Figure 4 displays the average performance of a machine learning model trained in a differentially private fashion with DP-FedAvg as a function of ϵ and δ . We compare it to a regular training using the same model initialization but without privacy (“Baseline wo DP”), trained with regular FedAvg. We see the performance diminishing when ϵ tends to 0, especially for small values of δ often used in practice, which is a standard phenomenon.

To implement DP in FedAvg, we use on the DP-SGD mechanism and track the monitoring of privacy budget thanks to the moment accountant [ACG⁺16]. We use the Opacus library [YSS⁺21], which is easy to integrate into FLamby thanks to its modular design.

At this time of writing, Opacus does not support all Deep Learning building blocks such as normalization layers. This prevents applying DP mechanisms on some some of FLamby’s baseline models such as the baseline for Fed-ISIC2019 and Fed-IXI.

L.2 Personalized Federated Learning

Model personalization [FMO20] is an effective strategy to improve model performance in cross-silo settings, especially in presence of data heterogeneity. Here, we showcase a simple example of model personalization with FLamby, which is possible thanks to its simple and modular API.

We implement the FedAvg strategy followed by local fine tuning on each center, thus producing as many models as there are clients. We test the addition of such fine-tuning process on the performances

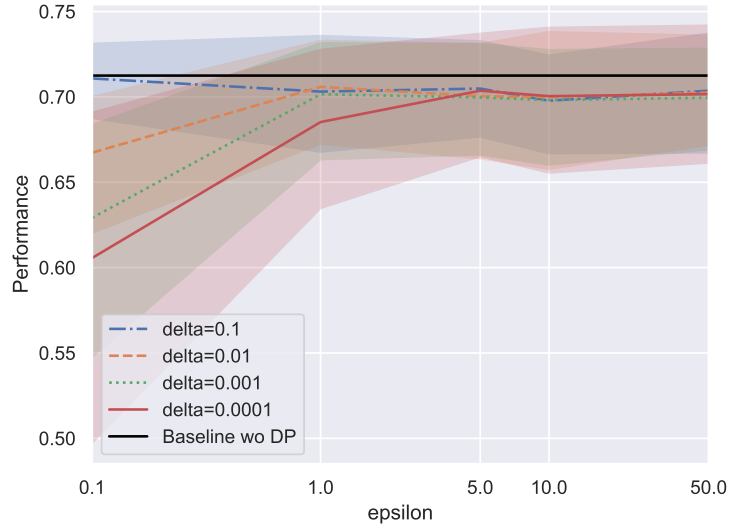


Figure 4: Impact of Differential-Privacy on average performance for DP-FedAvg on Fed-Heart-Disease.

of Federated models while testing each model on its corresponding test set. For each dataset, we perform 100 local updates after the federated averaging training has taken place.

Figure display the training results 5. We see that for Fed-Heart-Disease and Fed-ISIC2019, personalization improves results, while performance is slightly degraded for Fed-Camelyon16. We hope that researchers will be able to investigate more personalization strategies easily with FLamby.

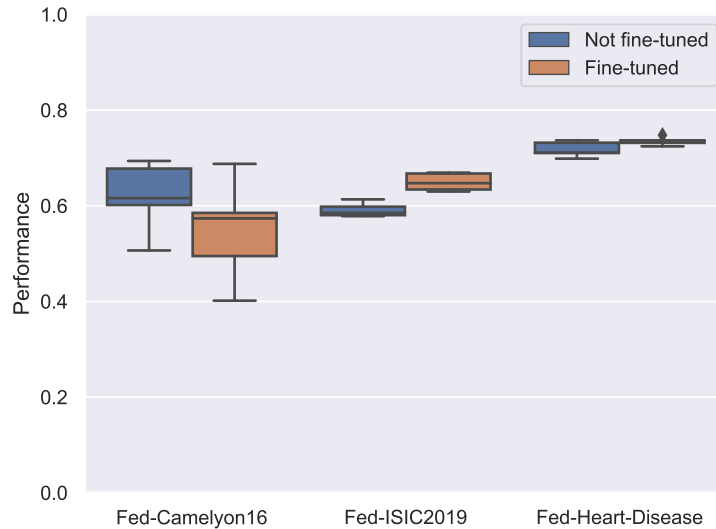


Figure 5: Impact of personalization on test average performance on three datasets of the suite (Fed-Heart-Disease, Fed-Camelyon16 and Fed-ISIC2019) after performing Federated Averaging. In the two extreme cases (Left and Right) fine-tuning is beneficial, whereas on Fed-Camelyon16, Fine-tuning degrades the performance of the resulting models. We hypothesize that, in this case, fine-tuning overfits the local training datasets.

M Quantitative heterogeneity benchmarks

We describe in this section our analysis of the heterogeneity of the Flamby datasets. Due to the variety of tasks and data, we restrict this study to generic metrics. We always compute them on the whole dataset, putting together test and train data to have the best possible estimation of the underlying distribution.

In the first subsection, we briefly describe the three sources of heterogeneity that we consider. Next, we detail the methodology used to compute statistical distance between clients. Thirdly, we apply this methodology to the FLamby’s dataset. And finally, we provide some discussion on these results.

M.1 Description of measured heterogeneity

Imbalance. The easiest quantification of heterogeneity comes from the number of samples hosted by each client, which gives natural unbalance in the training because small clients are likely to be either over-fitted or neglected in the final model.

Labels distribution. Labels can be another source of heterogeneity in case when prediction outputs vary between clients for the considered task. For instance, if a client is specialized in treating the patients with the given disease, the labels are likely to be biased (with a high number of persons with this disease), even if all clients have patients from a similar population. In the case of the toy example of MNIST, a split with this heterogeneity is to have clients specialized on a single digit.

Features distribution. Finally, in case when the features are the origin of heterogeneity, the underlying sample distribution is different in each client. It means that the same outputs can be characterized by different data depending on the client. This heterogeneity can arise from having different measurement tools (as is the case in Fed-LIDC-IDRI dataset), or different population in each client (e.g. Fed-TCGA-BRCA dataset). In the case of the toy example of MNIST, a split with this heterogeneity is to have a client where digits are in italics.

M.2 Methodology

For the sample division, we report the number of clients and the splits. As a way to summarize heterogeneity, we compute the entropy of the distribution of the samples across clients.

$$H(X) = - \sum_{k=1}^K \frac{n_k}{N} \log_2 \frac{n_k}{N} \tag{17}$$

where K is the number of clients, N the total number of samples and n_k the number of samples belonging to client k .

For label and features heterogeneity, when initial dimension is larger than 16, we reduce the dimension by using PCA trained on all the centralized samples. Then, for each client, we compute the Wasserstein distance (see Definition 1) between each client’s distribution, or the total variation distance (see Definition 2) for discrete data. The Wasserstein distances are computed using a minibatch-Wasserstein (without regularization) [see FZF⁺20] implemented in the POT library [FCG⁺21] and is defined below:

Definition 1 (Wasserstein distance) *For all probability measures α and β on $\mathcal{B}(\mathbb{R}^d)$, such that $\int_{\mathbb{R}^d} \|w\|^2 d\alpha(w) < +\infty$ and $\int_{\mathbb{R}^d} \|w\|^2 d\beta(w) \leq +\infty$, define the squared Wasserstein distance of order 2 between α and β by*

$$\mathcal{W}_2^2(\alpha, \beta) := \inf_{\xi \in \Gamma(\alpha, \beta)} \int \|x - y\|^2 \xi(dx, dy), \tag{18}$$

where $\Gamma(\alpha, \beta)$ is the set of probability measures ξ on $\mathcal{B}(\mathbb{R}^d \times \mathbb{R}^d)$ satisfying for all $A \in \mathcal{B}(\mathbb{R}^d)$, $\xi(A \times \mathbb{R}^d) = \beta(A)$, $\xi(\mathbb{R}^d \times A) = \alpha(A)$.

The Total-Variation distance used for discrete labels is defined as following:

Table 17: Mean and max distances for features and labels, and entropy computed using eq. 17. High values correspond to important heterogeneity.

	camelyon16	ixi	tcga brca	kits19	isic2019	heart disease
X mean	710618.57	188.52	6.38	-0.31	1.62	7.05
X max	710618.57	289.14	16.74	1.42	7.29	10.59
Y mean	-0.01	3.52	22.26	0.12	29.40	2.90
Y max	-0.01	6.95	79.42	2.68	53.87	5.77
Entropy	0.97	1.38	2.44	2.49	1.93	1.75

Definition 2 (Total-Variation) For any vector of probability α, β in $[0, 1]^d$, the TV-value is defined by

$$\text{TV}(\alpha, \beta) = \frac{1}{2} \sum_{i=1}^d |\alpha_i - \beta_i| \in [0, 1].$$

As the tasks, dimension and characteristics differs for each dataset, there are two directions to interpret results: 1) comparing heterogeneity between clients, and 2) by contrast with a synthetic scenario where data would be identically distributed among clients. Thus, we compute two pairwise-distances matrices: one with the natural split, and one with data distributed uniformly on clients (the size of the dataset on each client is identical to the natural split). The latter is built to simulate the i.i.d. setting and to compare the natural split with the case where we would have had homogeneous clients.

Next, we rescale the pairwise-distances matrices in order to have standardized variables in the synthetic case. Formally, we note $\mathcal{D}_{\text{i.i.d.}}$ (resp. $\mathcal{D}_{\text{natural}}$) the set of distances for the synthetic i.i.d. split (resp. natural split). The cardinal of these two sets is $n(n-1)/2$ because 1) the diagonal (distance of a client with itself) must be zero, 2) the Wasserstein distance is symmetric. Rescaling the matrices means that we standardize the i.i.d. set by removing the mean and scaling to unit variance i.e. computing $(\mathcal{D}_{\text{i.i.d.}} - \mu_{\text{i.i.d.}})/\sigma_{\text{i.i.d.}}$, where $\mu_{\text{i.i.d.}}, \sigma_{\text{i.i.d.}}^2$ are the mean and the variance of the i.i.d. set. Then, we apply the same transformation on the set of distance computed on the natural split i.e. $(\mathcal{D}_{\text{natural}} - \mu_{\text{i.i.d.}})/\sigma_{\text{i.i.d.}}$.

This is motivated by the fact that in the homogeneous case, we expect the distances to be zero. It follows that after rescaling, we are able to compare the values within the pairwise-distance matrix of the natural split. Thus, we are able to identify which clients are the closest or at odds with the others. Additionally, the magnitudes after rescaling give an indication on the degree of heterogeneity within the dataset. The bigger their magnitudes are after rescaling, the more distant is the natural split to what would be a homogeneous split.

M.3 Datasets analysis

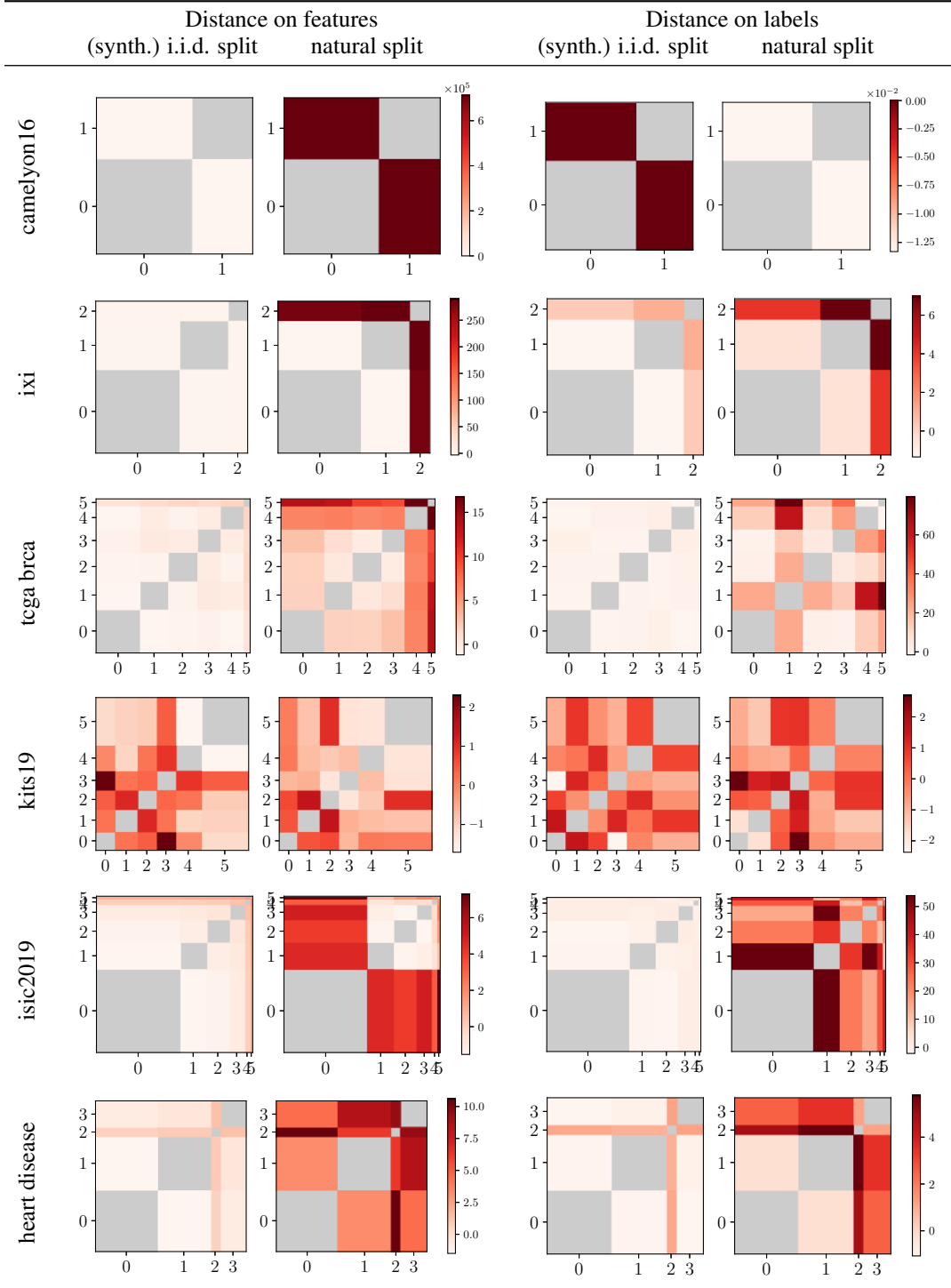
For each dataset, we report the rescaled pairwise-distances matrix for features and for labels, with the associated i.i.d. baseline in Figure 18. In order to highlight on the same plot the clients size imbalance and the clients' heterogeneity, the width of each column in the pairwise distance matrix is proportional to the client size. This helps to put heterogeneity in perspective with the size of the client and to have a better understanding of what is, in practice, the weight of the client's heterogeneity.

We also report the mean and maximum value for each dataset, both for features and labels, alongside sample distribution among client entropy in Table 17.

We can make the following observations for each dataset by analysing Tables 17 and 18.

- **Camelyon16.** There is a high heterogeneity on features, however labels are i.i.d.. This is of particular interest as it means that different features have led to close labels.
- **IXI.** Client 0 and 1 are very close, both in terms of features and labels. Compared to them, client 3 (which is also the smallest) is an outsider.
- **TCGA-BRCA.** In terms of features, clients 0, 1, 2, 3 are relatively close. But client 1 has labels different from the three other clients. Client 4 and 5 are apart, but it is interesting to

Table 18: Heterogeneity of Flamby datasets. Each matrix is the pairwise distance matrix, the width of their column corresponds to the number of sample.



notice that while their features are extremely different, their labels are almost identical. As for Camelyon16, this is of particular interest.

- **Kits19.** Clients are completely homogeneous for both features and labels. This can be derived from the fact that the distances are the same for both the natural split and the i.i.d. split. This was already suggested by Figure 1d.
- **Isic2019.** Features of client 0 are very different from the other clients. The four last clients have close features because their distances are almost zero. On the contrary, their distances on labels are far from zero. It means that close features have led to different labels. This is an element of particular interest.
- **Heart disease.** The heterogeneity on features and on labels are of the same order of magnitude (up to a factor 2) and not very important (maximum is at 10 for features, at 5 for labels). Client 2 is the smallest client and is an outsider. This is logical knowing that client 2 is a hospital specialized in major heart disease. We can also notice that client 1 and 2 have a moderate distance in terms of features. But however, based on their labels, they have the most significant distance. It means that relatively close features have led to very different labels. Like for isic2019, this is an element of particular interest. This could have happened if patients in hospital 2 have more severe heart disease than in other hospitals, but still have disease features close to classical cases.

M.4 Discussion

Measuring heterogeneity is an open question in machine learning, and it is beyond the scope of this paper. We provide some measurements as an indicative benchmark, with a methodology easy to reproduce. Other kind of heterogeneity could be computed and might lead to different conclusion on which clients are less or more similar, in particular as PCA representation can lead to a significant data loss. The advantages of this benchmark is its generality that allows to tackle the various data type and tasks found in FLamby.

References

- [ACG⁺16] Martin Abadi, Andy Chu, Ian Goodfellow, H Brendan McMahan, Ilya Mironov, Kunal Talwar, and Li Zhang. Deep learning with differential privacy. In *Proceedings of the 2016 ACM SIGSAC conference on computer and communications security*, pages 308–318, 2016.
- [AIMB⁺11] Samuel G Armato III, Geoffrey McLennan, Luc Bidaut, Michael F McNitt-Gray, Charles R Meyer, Anthony P Reeves, Binsheng Zhao, Denise R Aberle, Claudia I Henschke, Eric A Hoffman, et al. The lung image database consortium (LIDC) and image database resource initiative (IDRI): a completed reference database of lung nodules on ct scans. *Medical physics*, 38(2):915–931, 2011.
- [AMM⁺20] Mathieu Andreux, Andre Manoel, Romuald Menuet, Charlie Saillard, and Chloé Simpson. Federated survival analysis with discrete-time Cox models. *arXiv preprint arXiv:2006.08997*, 2020.
- [Aro] Aman Arora. Siim-isic melanoma classification - my journey to a top 5% solution and first silver medal on kaggle. <https://amaarora.github.io/2020/08/23/siim-isic.html>. Accessed: 2022-02-02.
- [Bra97] Andrew P Bradley. The use of the area under the roc curve in the evaluation of machine learning algorithms. *Pattern recognition*, 30(7):1145–1159, 1997.
- [CCR⁺19] Marc Combalia, Noel CF Codella, Veronica Rotemberg, Brian Helba, Veronica Vilaplana, Ofer Reiter, Cristina Carrera, Alicia Barreiro, Allan C Halpern, Susana Puig, et al. Bcn20000: Dermoscopic lesions in the wild. *arXiv preprint arXiv:1908.02288*, 2019.
- [CGC⁺18] Noel CF Codella, David Gutman, M Emre Celebi, Brian Helba, Michael A Marchetti, Stephen W Dusza, Aadi Kalloo, Konstantinos Liopyris, Nabin Mishra, Harald Kittler, et al. Skin lesion analysis toward melanoma detection: A challenge at the 2017

- international symposium on biomedical imaging (ISBI), hosted by the international skin imaging collaboration (ISIC). In *2018 IEEE 15th international symposium on biomedical imaging (ISBI 2018)*, pages 168–172. IEEE, 2018.
- [Cox72] David R Cox. Regression models and life-tables. *Journal of the Royal Statistical Society: Series B (Methodological)*, 34(2):187–202, 1972.
- [CVS+13] Kenneth Clark, Bruce Vendt, Kirk Smith, John Freymann, Justin Kirby, Paul Koppel, Stephen Moore, Stanley Phillips, David Maffitt, Michael Pringle, et al. The cancer imaging archive (TCIA): maintaining and operating a public information repository. *Journal of digital imaging*, 26(6):1045–1057, 2013.
- [DCM+20] Olivier Dehaene, Axel Camara, Olivier Moindrot, Axel de Lavergne, and Pierre Courtiol. Self-supervision closes the gap between weak and strong supervision in histology. *arXiv preprint arXiv:2012.03583*, 2020.
- [DG17] Dheeru Dua and Casey Graff. UCI machine learning repository, 2017.
- [Dic45] Lee R Dice. Measures of the amount of ecologic association between species. *Ecology*, 26(3):297–302, 1945.
- [DR+14] Cynthia Dwork, Aaron Roth, et al. The algorithmic foundations of differential privacy. *Found. Trends Theor. Comput. Sci.*, 9(3-4):211–407, 2014.
- [dt] Brain development team. Ixi dataset. <https://brain-development.org/ixi-dataset/>. Accessed: 2022-02-02.
- [FCG+21] Rémi Flamary, Nicolas Courty, Alexandre Gramfort, Mokhtar Z. Alaya, Aurélie Boisbunon, Stanislas Chambon, Laetitia Chapel, Adrien Corenflos, Kilian Fatras, Nemo Fournier, Léo Gautheron, Nathalie T.H. Gayraud, Hicham Janati, Alain Rakotomamonjy, Ievgen Redko, Antoine Rolet, Antony Schutz, Vivien Seguy, Danica J. Sutherland, Romain Tavenard, Alexander Tong, and Titouan Vayer. POT: Python optimal transport. *Journal of Machine Learning Research*, 22(78):1–8, 2021.
- [FDZ+15] Christopher P Favazza, Xinhui Duan, Yi Zhang, Lifeng Yu, Shuai Leng, James M Kofler, Michael R Bruesewitz, and Cynthia H McCollough. A cross-platform survey of ct image quality and dose from routine abdomen protocols and a method to systematically standardize image quality. *Physics in Medicine & Biology*, 60(21):8381, 2015.
- [Fee10] Timothy G Feeman. *The mathematics of medical imaging*. Springer, 2010.
- [FMO20] Alireza Fallah, Aryan Mokhtari, and Asuman Ozdaglar. Personalized federated learning: A meta-learning approach. *arXiv preprint arXiv:2002.07948*, 2020.
- [FZF+20] Kilian Fatras, Younes Zine, Rémi Flamary, Rémi Gribonval, and Nicolas Courty. Learning with minibatch Wasserstein : asymptotic and gradient properties. In *AISTATS 2020 - 23rd International Conference on Artificial Intelligence and Statistics*, volume 108 of *PMLR*, pages 1–20, Palermo, Italy, June 2020.
- [GNS+19] Nils Gessert, Maximilian Nielsen, Mohsin Shaikh, René Werner, and Alexander Schlaefer. Skin lesion classification using ensembles of multi-resolution efficientnets with meta data. *CoRR*, abs/1910.03910, 2019.
- [Goo92] Irving John Good. Rational decisions. In *Breakthroughs in statistics*, pages 365–377. Springer, 1992.
- [HIMH+20] Nicholas Heller, Fabian Isensee, Klaus H Maier-Hein, Xiaoshuai Hou, Chunmei Xie, Fengyi Li, Yang Nan, Guangrui Mu, Zhiyong Lin, Miofei Han, et al. The state of the art in kidney and kidney tumor segmentation in contrast-enhanced ct imaging: Results of the kits19 challenge. *Medical Image Analysis*, page 101821, 2020.

- [HSK⁺19] Nicholas Heller, Niranjana Sathianathan, Arveen Kalapara, Edward Walczak, Keenan Moore, Heather Kaluzniak, Joel Rosenberg, Paul Blake, Zachary Rengel, Makinna Oestreich, et al. The kits19 challenge data: 300 kidney tumor cases with clinical context, ct semantic segmentations, and surgical outcomes. *arXiv preprint arXiv:1904.00445*, 2019.
- [HZRS16] Kaiming He, Xiangyu Zhang, Shaoqing Ren, and Jian Sun. Deep residual learning for image recognition. In *Proceedings of the IEEE conference on computer vision and pattern recognition*, pages 770–778, 2016.
- [IJK⁺21] Fabian Isensee, Paul F Jaeger, Simon AA Kohl, Jens Petersen, and Klaus H Maier-Hein. nnu-net: a self-configuring method for deep learning-based biomedical image segmentation. *Nature methods*, 18(2):203–211, 2021.
- [ILTT11] Juan Eugenio Iglesias, Cheng-Yi Liu, Paul M Thompson, and Zhuowen Tu. Robust brain extraction across datasets and comparison with publicly available methods. *IEEE transactions on medical imaging*, 30(9):1617–1634, 2011.
- [IMB⁺15] S. G. Armato III, G. McLennan, L. Bidaut, M. F. McNitt-Gray, C. R. Meyer, A. P. Reeves, B. Zhao, D. R. Aberle, C. I. Henschke, E. A. Hoffman, E. A. Kazerooni, H. MacMahon, E. J. R. Van Beek, D. Yankelevitz, A. M. Biancardi, P. H. Bland, M. S. Brown, R. M. Engelmann, G. E. Laderach, D. Max, R. C. Pais, D. P. Y. Qing, R. Y. Roberts, A. R. Smith, A. Starkey, P. Batra, P. Caligiuri, A. Farooqi, G. W. Gladish, C. M. Jude, R. F. Munden, I. Petkovska, L. E. Quint, L. H. Schwartz, B. Sundaram, L. E. Dodd, C. Fenimore, D. Gur, N. Petrick, J. Freymann, J. Kirby, B. Hughes, A. V. Castele, S. Gupte and M. Sallam, M. D. Heath, M. H. Kuhn, E. Dharaiya, R. Burns, D. S. Fryd, M. Salganicoff, V. Anand, U. Shreter, S. Vastagh, B. Y. Croft, and L. P. Clarke. Data from lidc-idri [data set]. the cancer imaging archive., 2015.
- [ITW] Maximilian Ilse, Jakub M. Tomczak, and Max Welling. Attention-based deep multiple instance learning. <https://github.com/AMLab-Amsterdam/AttentionDeepMIL>. Accessed: 2022-02-02.
- [Jad20] Shruti Jadon. A survey of loss functions for semantic segmentation. In *2020 IEEE Conference on Computational Intelligence in Bioinformatics and Computational Biology (CIBCB)*, pages 1–7. IEEE, 2020.
- [Jen05] Stephen P Jenkins. Survival analysis. *Unpublished manuscript, Institute for Social and Economic Research, University of Essex, Colchester, UK*, 42:54–56, 2005.
- [JSPD88] Andras Janosi, William Steinbrunn, Matthias Pfisterer, and Robert Detrano. Heart disease data set, 1988.
- [KB14] Diederik P Kingma and Jimmy Ba. Adam: A method for stochastic optimization. *arXiv preprint arXiv:1412.6980*, 2014.
- [LBEB⁺18] Geert Litjens, Peter Bandi, Babak Ehteshami Bejnordi, Oscar Geessink, Maschenka Balkenhol, Peter Bult, Altuna Halilovic, Meyke Hermsen, Rob van de Loo, Rob Vogels, et al. 1399 H&E-stained sentinel lymph node sections of breast cancer patients: the CAMELYON dataset. *GigaScience*, 7(6):guy065, 2018.
- [LGG⁺17] Tsung-Yi Lin, Priya Goyal, Ross B. Girshick, Kaiming He, and Piotr Dollár. Focal loss for dense object detection. *CoRR*, abs/1708.02002, 2017.
- [LLH⁺18] Jianfang Liu, Tara Lichtenberg, Katherine A Hoadley, Laila M Poisson, Alexander J Lazar, Andrew D Cherniack, Albert J Kovatich, Christopher C Benz, Douglas A Levine, Adrian V Lee, et al. An integrated tcga pan-cancer clinical data resource to drive high-quality survival outcome analytics. *Cell*, 173(2):400–416, 2018.
- [MAB] Alessia Marcolini, Ernesto Arbitrio, and Nicole Bussola. <https://histolab.readthedocs.io/en/latest/>. <https://histolab.readthedocs.io/en/latest/>. Accessed: 2022-05-18.

- [MLI⁺14] Matthew McCormick, Xiaoxiao Liu, Luis Ibanez, Julien Jomier, and Charles Marion. Itk: enabling reproducible research and open science. *Frontiers in Neuroinformatics*, 8, 2014.
- [MNA16] Fausto Milletari, Nassir Navab, and Seyed-Ahmad Ahmadi. V-net: Fully convolutional neural networks for volumetric medical image segmentation. In *2016 fourth international conference on 3D vision (3DV)*, pages 565–571. IEEE, 2016.
- [Mod] Marc Modat. Nifty reg. <https://sourceforge.net/p/niftyreg/git/ci/master/tree/>. Accessed: 2022-02-02.
- [Net] TCGA Research Network. Tensorflow federated stack overflow dataset. <https://www.cancer.gov/tcga>. Accessed: 2022-05-18.
- [PG] Fernando Pérez-García. Ixitiny dataset. <https://torchio.readthedocs.io/datasets.html#torchio.datasets.ixi.IXITiny>. Accessed: 2022-05-18.
- [PGM⁺19] Adam Paszke, Sam Gross, Francisco Massa, Adam Lerer, James Bradbury, Gregory Chanan, Trevor Killeen, Zeming Lin, Natalia Gimelshein, Luca Antiga, et al. Pytorch: An imperative style, high-performance deep learning library. *Advances in neural information processing systems*, 32, 2019.
- [RFB15] Olaf Ronneberger, Philipp Fischer, and Thomas Brox. U-net: Convolutional networks for biomedical image segmentation. In *International Conference on Medical image computing and computer-assisted intervention*, pages 234–241. Springer, 2015.
- [TL19] Mingxing Tan and Quoc V. Le. Efficientnet: Rethinking model scaling for convolutional neural networks. *CoRR*, abs/1905.11946, 2019.
- [TRK18] Philipp Tschandl, Cliff Rosendahl, and Harald Kittler. The HAM10000 dataset, a large collection of multi-source dermatoscopic images of common pigmented skin lesions. *Scientific data*, 5(1):1–9, 2018.
- [VDWCV11] Stefan Van Der Walt, S Chris Colbert, and Gael Varoquaux. The numpy array: a structure for efficient numerical computation. *Computing in science & engineering*, 13(2):22–30, 2011.
- [WLL⁺20] Wenqi Wei, Ling Liu, Margaret Loper, Ka-Ho Chow, Mehmet Emre Gursoy, Stacey Truex, and Yanzhao Wu. A framework for evaluating gradient leakage attacks in federated learning. *arXiv preprint arXiv:2004.10397*, 2020.
- [YAG⁺19] Mikhail Yurochkin, Mayank Agarwal, Soumya Ghosh, Kristjan Greenewald, Nghia Hoang, and Yasaman Khazaeni. Bayesian nonparametric federated learning of neural networks. In *International Conference on Machine Learning*, pages 7252–7261. PMLR, 2019.
- [YSS⁺21] Ashkan Yousefpour, Igor Shilov, Alexandre Sablayrolles, Davide Testuggine, Karthik Prasad, Mani Malek, John Nguyen, Sayan Ghosh, Akash Bharadwaj, Jessica Zhao, et al. Opacus: User-friendly differential privacy library in pytorch. *arXiv preprint arXiv:2109.12298*, 2021.